by

George Leonard Tyler, Jr.

May 1967

Scientific Report No. 19

RADIOSCIENCE LABORATORY

STANFORD ELECTRONICS LABORATORIES

STANFORD UNIVERSITY · STANFORD, CALIFORNIA

BISTATIC-RADAR IMAGING AND MEASUREMENT TECHNIQUES
FOR THE STUDY OF PLANETARY SURFACES

by

George Leonard Tyler, Jr.

May 1967

Radioscience Laboratory
Stanford Electronics Laboratories
Stanford University   Stanford, California

ABSTRACT

The problem of imaging a planetary surface is considered from the point of view of continuous wave bistatic-radar in which transmissions originating on the Earth (or on a spacecraft) would be received on a spacecraft (or on the Earth) after reflection from a planetary surface.

An electromagnetic wave reflected by a planet may be considered as a superposition of the waves from elementary scatterers on the surface. Using a superposition model the ordinary radar brightness distribution, the differential radar cross-section, the polar scattering diagram, and the radar albedo of a surface are all related measures of the local surface properties.

The surface brightness distribution may be determined by cross-correlating the scattered fields (as measured by a spacecraft along some fraction of its trajectory) with the expected signal from each point on the surface. The predicted azimuthal resolution in wavelengths is inversely proportional to the angle subtended at the target point by the fraction of the trajectory over which the data are taken; in range the resolution in wavelengths is inversely proportional to the square of the same angle. The feasibility of the method depends on the use of the illuminating wave on board the spacecraft as a frequency reference to achieve the requisite stability.

Physical analogs of the process exist as modifications of holograms and synthetic antenna arrays. An additional analog is that of a bank of tracking filters, each of which is adjusted to receive the signals from a separate portion of the surface.

The maximum-likelihood estimator for the brightness of a specific scattering area, in the presence of white Gaussian noise at low input signal-to-noise ratios, is a Hilbert quadratic form with the expected autocorrelation function of the signal from the scattering area as a

kernel. For maximum resolution (minimum area) this is equivalent to the cross-correlation method for obtaining the brightness distribution. Furthermore, this estimate is efficient in the sense of being unbiased and of having minimum variance, for the low signal-to-noise ratio case.

The estimator may be realized with well-known forms of time-varying or time-invariant filters, or with correlators. A new realization is that of a hologram scanned with a properly weighted illuminating wave.

It is concluded that bistatic-radars operating between a ground station and a vehicle in space constitute a powerful technique with which to map and to study planetary surfaces.

CONTENTS

CONTENTS (Cont)

ILLUSTRATIONS

ILLUSTRATIONS (Cont)

SYMBOLS

a	**complex amplitude of point scatter**
$\hat{a}$	estimate of a
$c(t)$	analytic representation of autocorrelation function
$\tilde{e}_s(\bar{r})$	analytic representation of scattered wave
f	Fresnel number
$f(\omega)$	narrowband frequency spectrum
F	complex envelope of scattering kernel
$g_v(\bar{u})$	antenna voltage gain in direction $-\bar{u}$
j	$(-)^{1/2}$
k	$\|\bar{k}\| = 2\pi/\lambda$ wave number
$\bar{k}$	wave vector
$n(t)$	Gaussian random process
$\tilde{n}(t)$	analytic representation of $n(t)$
$\bar{p}$	position vector
$\bar{r}$	position vector
r	distance, usually $\|\bar{p} - \bar{r}\|$
$s(t)$	real signal
$\bar{s}(t)$	position vector
t	independent time variable
$\bar{u}$	unit vector
$x(t)$	real part of analytic representation of $z(t)$
$y(t)$	imaginary part of analytic representation of $z(t)$
$z(t)$	analytic representation of $s(t)$
A	average surface current

A^2	average surface brightness
A_r	area of receiving antenna
$\overline{A}$	magnetic vector potential
$B(\overline{r})$	surface brightness distribution
$C(\tau)$	complex envelope of autocorrelation function
E	energy
$E(\ )$	even functions
$E(r)$	complex envelope of scalar component of electric field
$\overline{E}_s(\overline{r})$	complex envelope of scattered electric field vector
G_T	gain of transmitting antenna
$G(\omega)$	complex envelope filter transfer function
$\overline{H}(\overline{r})$	complex envelope magnetic field intensity
$\overline{J}(\overline{r})$	complex envelope of volume current distribution
$\overline{K}(\overline{r})$	analytic representation of surface current distribution
$K(\overline{r})$	scalar component of C.E. of surface current distribution
$M(t)$	amplitude of $Z(t)$
$N(t)$	complex envelope of noise waveform
$O(\ )$	odd function
P_R	received power
P_T	transmitted power
R	distance of closest approach
R_1	range, transmitter to target
R_2	range, target to receiver
$S(\omega)$	transform of $s(t)$
S'	surface of integration
V'	volume of integration

$X(t)$	in-phase component of $Z(t)$
$X_n(t)$	in-phase component of $N(t)$
$Y(t)$	quadrature component of $Z(t)$
$Y_n(t)$	quadrature component of $N(t)$
$Z(t)$	complex envelope of $s(t)$

α_1, α_o	angular limits of data path
$\delta(\rho)$	Dirac delta function
ϵ	dielectric constant
$\epsilon(s)$	error function
ζ	path length
η	independent surface coordinate perpendicular to trajectory
θ_i	angle of incidence
θ_p	angle between planes of incidence and reflection
θ_r	angle of reflection
λ	wavelength
μ	permeability
$\left.\begin{array}{c}\mu\\ \nu\end{array}\right\}$	summation index
ξ	independent surface coordinate parallel to trajectory
ρ	radial space coordinate
$\rho(\varphi_i)$	albedo
σ	radar cross section
σ^o	differential radar cross section
τ	independent time variable

υ	angular error in trajectory
$\varphi(\tau)$	autocorrelation function of $N(t)$
$\phi(t)$	phase of $Z(t)$
ψ	phase difference
ω	radian frequency
Δ	difference coordinate
H	$(\eta_1 - \eta_0)$
$\Lambda(\rho)$	normalized integrated response function
Ξ	$(\xi_1 - \xi_0)$
$\Phi(\omega)$	power spectral density
$\Phi(\bar{r})$	electric scalar potential
$\psi(\theta_r, \theta_p; \theta_i)$	polar scattering diagram
Ω	radian frequency

ACKNOWLEDGMENT

I. INTRODUCTION

A. STIMULUS FOR THIS RESEARCH

The first radars, dating from experiments at the turn of the century were bistatic in their operation.[1,2*] That is, they were radars in which the transmitter and receiver occupied not the same, but two separate, remote, and generally fixed positions. Energy was continuously radiated from the transmitting site, and target detection relied upon scattering enough of the transmitted signal power into the receiving antenna by the target to overcome the noise of the receiving system. The receiving sites were usually effectively shielded from the transmitter, and target detection was signaled by an increase in the power output of the receiver. An alternative was to allow a small amount of power from the transmitter to leak directly into the receiver. In this second case a Doppler-shifted signal from a moving target appeared as a beat note at the Doppler frequency. By the early 1930s, enough progress had been made to permit the detection of aircraft at ranges of a few tens of miles.[1]

Now, three decades later, astronomical bistatic radars, employing transmissions between a station on the ground and a receiver on board a spacecraft in interplanetary space, are being used as a scientific tool to probe the electromagnetic properties of the intervening medium. These experiments are characterized by the continuous presence at the receiver of a strong signal, directly from the transmitter, which is examined for perturbations in phase, amplitude, or polarization introduced by material along the path followed by the wave.[3] Independent measurements of two or more of these signal characteristics made simultaneously on several frequencies may be employed to magnify the effects of the medium and to calibrate the experiment.[3]

The concept of bistatic-radar for probing tenuous astronomical media was quickly extended to include proposed experiments for determining the properties of planetary atmospheres and ionospheres.[4,5] Here the experimenter makes use of his control over the spacecraft trajectory. By causing the spacecraft to pass behind the planet, the propagation path between the

---

*References are listed at the end of the report.

ground station and the vehicle is forced to slice through whatever surrounding medium there may be. Since the spacecraft's position with respect to the planet is well known, it is possible to associate the measurements with particular paths through the medium and consequently with particular portions of the atmosphere. The data obtained, together with certain auxiliary information, are then used to establish the salient physical and chemical properties of the atmosphere and ionosphere involved.[6,7]

The next possibility is immediately clear: A spacecraft may serve as one terminal of a bistatic-radar system for exploring the surface of a planet. Either transmissions from the earth would be directed at the planet and the scattered energy would be received on board the vehicle, or energy directed toward the planet by the spacecraft would be received on the ground after scattering from the surface. There are several reasons to believe this will be useful.

1. Relative to purely passive observations, the probing signal is under the experimenter's control, and its characteristics may be chosen to maximize the experimental sensitivity to a given surface property.

2. Relative to ground-based radars, (a) one leg of the radar path may be made very short, thus increasing the signal strength at the receiver, and (b) the angles of incidence and reflection are variable, thus allowing the resolution of the surface-scattering properties as a function of direction.

3. Relative to on-board radars, only a transmitter or a receiver is required thus considerably reducing the weight, power consumption, and complexity of the spaceborne equipment. If this advantage is to be realized, then only one-way transmissions may be used for the experiment: signals may go from the spacecraft to the ground or vice versa. Data stored on the spacecraft will be retrievable by telemetry.

4. Relative to optical measurements, radar may be the only means for observing the surface of Venus for some time.

5. Signals reflected from the surface may be needed to remotely probe the atmospheres of some planets below a critical refraction level.

This research was instigated to determine if there were ways in which the bistatic technique could be used, extended, or modified to realize the potentials listed above for the study of planetary surfaces.

B. PREVIOUS CONTRIBUTIONS

It is not clear who first suggested the bistatic-radar approach to planetary surface studies. To this author's knowledge, the first written comments were in a January 1961 memorandum, by Evans and Pettengill,[8] in which they discussed the limitations of monostatic radar for surface studies and means of resolving these difficulties with bistatic-radar probes. Their suggestion was to transmit with an omni-directional antenna from a vehicle orbiting the Moon and to receive the scattered energy with a tunable radiometer. In effect, they would rely upon strong quasi-specular scattering to isolate a fraction of the disk and resolve the mono-static scattering law ambiguities.

The second written contribution evidently came from a NASA study group convened for the purpose of discussing bistatic-radar, with the result that the potential advantages listed in the introduction were articulated in the group's report, which was authored by Eshleman.[9] What is important here is that the application of bistatic-radar was realized to be a versatile and potentially powerful tool for planetary exploration.

Finally, in a work dealing primarily with bistatic probing of planetary atmospheres, Fjeldbo[4] derived the properties of the quasi-specular scattering from a surface as seen from a space probe, and related the spectral characteristics of the scattered signal to the parameters of a surface generated by a stationary Gaussian process.

There have also been several papers and reports on the degradation of communications systems caused by reflections from planetary surfaces by extrapolation of monostatic radar results.

In addition to the work above, there were a number of meetings and conferences[10], beginning in June 1960, when the general topic of bistatic-radar for astronomical studies was introduced by V. R. Eshleman. Several proposals for studies of the use of lunar orbiters and planetary flybys were initiated at Stanford Univeristy in 1962.

The first bistatic-radar experiments for the study of the surface of a celestial body were carried out in October 1966, by the author, in collaboration with his colleagues at the Center for Radar Astronomy, Stanford University.[11]

C. DESCRIPTION OF PRESENT WORK

The present work proceeds along the following lines.

Chapter II is a general examination of the scattering properties of a planet as viewed from a spacecraft. The analytic signal representation of the scattered wave is introduced, a simple integral representation of the scattered wave is derived in terms of the analytic signal, and the radar brightness distribution is defined. The connection between this formulation and the more common radar cross-section and polar scattering diagram is given next. Specific features of the scattered fields as received on board a spacecraft are given last.

Chapter III deals with a method for recovering the radar brightness distribution from the scattered wave on the basis of a heuristic argument. The resolution cell, signal-to-noise ratio, and sensitivity to errors are determined for this method. It is also shown how the method may be made self-calibrating by use of the illuminating wave as a reference signal.

Chapter IV gives three physical interpretations of the inversion method. First, it is considered as a synthetic array, performing as an antenna focused in its own near-field. Second, we give an interpretation as a tracking filter and explain the resolution properties in terms of the filter characteristics. Third, we develop an analogy with holograms, and show how the inversion may be automatically realized with a properly constructed diffracting screen.

Chapter V develops the inversion as a maximum-likelihood estimator of the brightness distribution from a specified surface area. The general form of the estimator is derived. Then after restricting the problem to low input signal-to-noise ratios, the estimator is applied to the inversion problem. It is shown that the process produces an unbiased minimum variance estimate of the surface brightness distribution. The relationship between the variance of the estimate of the surface brightness and the size and shape of our resolution cell is investigated in the last section.

Chapter VI presents five methods of realizing the estimator. Realization in terms of two time-invariant filters (one physically realizable and one not physically realizable), a time-varying filter, and an autocorrelator are given. The realization of the optimum filter through the hologram analog is also discussed.

Chapter VII gives some experimental results from the first application of bistatic-radar to the surface of a celestial body. An experiment using Lunar Orbiter spacecraft is described and some samples of the observations are given. A two-dimensional map, made from observation of a reflected, continuous-wave signal, is presented.

Chapter VIII gives the conclusions we might reach from the preceding seven chapters.

The author has made the following contributions to this research:

1. A method for the two-dimensional bistatic-radar mapping of planetary surfaces using a continuous-wave mode of transmission between the Earth and a spacecraft.

2. An analysis of that method based upon techniques from conventional radar and optical imaging theory.

3. Three analog interpretations of the method in terms familiar devices.

4. The derivation of a specific maximum-likelihood estimator for the radar brightness of a general scattering area from data taken on a moving spacecraft. The conditions under which the original method is optimum and the means by which it should be modified for other conditions are determined.

5. The first bistatic-radar measurements of the scattering properties of the Moon, and the preliminary reduction of the data in terms of the ideas developed above.

SEL-67-042

II. PHYSICAL ASSUMPTIONS AND DESCRIPTION OF THE SCATTERED WAVE

A. THE ANALYTIC SIGNAL

The use of complex numbers to describe real physical processes is a familiar tool of scientists and engineers. Sinusoidal analysis in the time domain frequently makes use of the relations

$$\cos \Omega t = R_\ell \{e^{j\Omega t}\}$$

and   (2.1)

$$\sin \Omega t = I_m \{e^{j\Omega t}\}$$

to interpret a real oscillation as the projection of a rotating phasor onto a fixed axis. Similarly, complex Fourier analysis exploits

$$\cos \Omega t = \frac{e^{j\Omega t} + e^{-j\Omega t}}{2}$$

and   (2.2)

$$\sin \Omega t = \frac{e^{j\Omega t} - e^{-j\Omega t}}{2j}$$

to decompose real functions into complex integrals over frequency.

While these formulations have great merit, both in a mathematical sense and in the physical insight they afford, they are somewhat awkward for dealing with signals when time-frequency dependence is important.

In this report we will be dealing extensively with time changes in relative phase among a group of signals. Consequently, the analytic signal, a formalized, time-varying version of the rotating phasor, is introduced. This device will allow us to deal explicitly with the relative phases of signals, and the time variations of phases. The presentation here is

standard,[12] although in what follows we shall try to emphasize the features of this representation which will be of use to us later. A few elementary results from communication theory will be stated as they apply.

We shall consider a real signal $s(t)$ with Fourier spectrum $S(\omega)$, so that

$$S(\omega) = \int_{-\infty}^{\infty} s(t) e^{-j\omega t} dt$$

and (2.3)

$$s(t) = \frac{1}{2\pi} \int_{-\infty}^{\infty} S(\omega) e^{j\omega t} d\omega$$

As a direct consequence of $s(t)$ real we have

$$S(-\omega) = S(\omega)^*$$ (2.4)

where the asterisk is used to denote the complex conjugate. Hence, nothing is lost if we consider only $S(\omega)$ for $\omega \geq 0$, since the function of the negative argument may always be recovered from its value along the positive real axis.

The time function generated by transforming the truncated spectrum obtained by discarding $S(\omega)$ for $\omega < 0$ and doubling the remainder is the analytic signal

$$z(t) = \frac{1}{\pi} \int_0^{\infty} S(\omega) e^{j\omega t} d\omega = x(t) + jy(t)$$ (2.5)

The function $z(t)$ is not real, but its real part, $x(t)$, is the original $s(t)$, as may be shown by

$$z^*(t) = \frac{1}{\pi} \int_0^{\infty} S^*(\omega) e^{-j\omega t} d\omega = \frac{1}{\pi} \int_{-\infty}^0 S(\omega) e^{j\omega t} d\omega$$ (2.6)

SEL-67-042

$$s(t) = \frac{1}{2\pi} \int_{-\infty}^{+\infty} S(\omega) \; e^{j\omega t} \; d\omega = \frac{z(t) + z^*(t)}{2} = R_\ell\{z(t)\} \qquad (2.7)$$

or $s(t) = x(t)$.

Eq. 2.5 allows us to interpret $z(t)$ as a collection of infinitesimal phasors, the $e^{j\omega t} d\omega$, rotating in the same direction, albeit at different ω, with respective amplitudes $S(\omega)$. If $s(t)$ is considered as a narrow-band signal with spectrum $S(\omega)$ which is non-zero only about some frequency Ω, this interpretation becomes quite clear. For example, take

$$S(\omega) = f(\omega - \Omega) + f^*(-\omega - \Omega), \qquad f(\omega) = 0 \quad \text{for} \quad |\omega| > W$$
$$W < \Omega \qquad (2.8)$$

as a representation of a narrow-band signal. The analytic signal becomes

$$z(t) = \frac{1}{\pi} \int_0^\infty S(\omega) \; e^{j\omega t} \; d\omega = \frac{1}{\pi} \int_{-\Omega}^\infty f(\omega) \; e^{j(\omega + \Omega)t} \; d\omega$$
$$(2.9)$$
$$= e^{j\Omega t} \frac{1}{\pi} \int_{-W}^{+W} f(\omega) \; e^{j\omega t} \; d\omega = Z(t) \; e^{j\Omega t}$$

As before,

$$s(t) = R_\ell\{z(t)\} = R_\ell\{Z(t) \; e^{j\Omega t}\} \qquad (2.10)$$

Writing $Z(t) = X(t) + j \, Y(t)$, we have

$$s(t) = X(t) \cos \Omega t - Y(t) \sin \Omega t \qquad (2.11)$$

The $X(t)$ and $Y(t)$ are referred to as the in-phase and quadrature components of $s(t)$. The complex envelope of $s(t)$ is $Z(t)$. It should be noted that Ω has been specified in only the most general terms, and that the form of these results is not critically dependent on the value of Ω, even though the exact $Z(t)$ obtained may be. In addition, $Z(t)$, and

X(t) and Y(t) likewise, are relatively slowly varying functions that change significantly only in a time greater than 1/W.

In terms of Eq. 2.5 we have separated $z(t)$ into a reference phasor or carrier of constant frequency and amplitude, $e^{j\Omega t}$, and a complex modulating function $Z(t)$ of amplitude

$$M(t) = \{X^2(t) + Y^2(t)\}^{\frac{1}{2}}$$

and angle

$$\phi(t) = \tan^{-1}\left\{\frac{Y(t)}{X(t)}\right\} \tag{2.12}$$

From now on the term phase will refer specifically to a function $\phi(t)$; amplitude will refer to $M(t)$. In particular if $M(t)$ is constant, so that we have a purely phase-modulated wave, we picture the signal as a phasor spinning in the complex plane with the nominal angular position (phase) Ωt and gaining or losing by the quantity $\phi(t)$. The representation of $\cos(\Omega t - \phi(t))$ is simply $e^{j(\Omega t - \phi(t))}$. This concept will be important to us later.

A distinct virtue of this formulation is the ease with which $X(t)$ and $Y(t)$ may be obtained by measurement. If we multiply $s(t)$ by $\cos \Omega t$ the result is

$$s(t) \cos \Omega t = \frac{1}{2} X(t) + \frac{1}{2} X(t) \cos 2\Omega t - \frac{1}{2} Y(t) \sin 2\Omega t \tag{2.13}$$

Removing the $2\Omega t$ terms by filtering and doubling the resultant gives $X(t)$. A similar procedure employing $\sin \Omega t$ yields $Y(t)$. A block diagram for this operation is given in Fig. 1. The cutoff frequency for the filter, ω_c, need only be low enough to avoid the twice-frequency terms in Eq. 2.13, and high enough to pass all of $X(t)$ and $Y(t)$. Generally, it is advantageous to use the lowest possible value consistent with the modulation bandwidth.

SEL-67-042
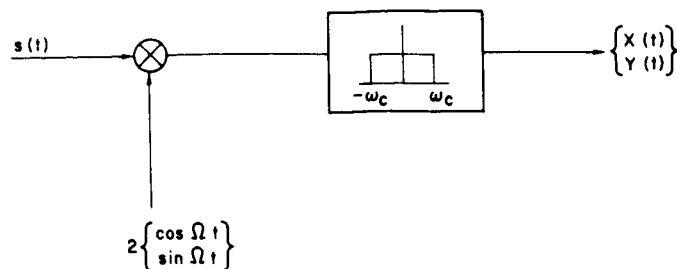
FIG. 1. METHOD FOR OBTAINING COMPLEX ENVELOPE.

We may also relate $z(t)$ to the energy E in the signal. From Parseval's theorem

$$E = \frac{1}{2\pi} \int_{-\infty}^{+\infty} |S(\omega)|^2 \, d\omega = \int_{-\infty}^{+\infty} s^2(t) \, dt \qquad (2.14)$$

and

$$\int_{-\infty}^{+\infty} |S(\omega)|^2 \, d\omega = 2 \int_{0}^{\infty} |S(\omega)|^2 \, d\omega \quad \text{for} \quad S(-\omega) = S^*(\omega) \qquad (2.15)$$

and since $x(t) = s(t)$ we have

$$E = \int_{-\infty}^{+\infty} x^2(t) \, dt = \int_{-\infty}^{+\infty} y^2(t) \, dt = \frac{1}{2} \int_{-\infty}^{+\infty} |z(t)|^2 \, dt \qquad (2.16)$$

If we now consider filters with real impulse response $h(\tau)$, and transfer functions $H(\omega)$, it follows that we may define a complex impulse response

$$g(\tau) = \frac{1}{\pi} \int_{0}^{\infty} H(\omega) \, e^{j\omega\tau} \, d\omega \qquad (2.17)$$

As before, we have generated the complex representations by discarding the spectrum for $\omega < 0$ and doubling the resultant. By restricting the problems to narrow-band filters about Ω, we again have

$$g(\tau) = G(\tau) \, e^{j\Omega\tau} \qquad (2.18)$$

with $G(t)$ the complex envelope function of the filter response in a manner completely analogous to $z(t)$ and $Z(t)$. Still with the narrow-band restriction and letting $s_i(t)$ and $s_0(t)$ be the input and output signals respectively of $h(t)$,

$$s_0(t) = \int_{-\infty}^{\infty} h(\tau) \, s_i(t-\tau) \, d\tau \qquad (2.19)$$

It is a simple matter to show that

$$z_0(t) = e^{j\Omega t} \int_{-\infty}^{+\infty} G(\tau) \, z_i(t-\tau) \, d\tau \qquad (2.20)$$

where $z_0(t)$ is the complex envelope of the analytic response function of the filter. Thus, the complex envelope of the response of a narrow-band filter to a narrow-band signal may be calculated directly from the complex envelopes of the input signal and the impulse response function of the filter. It is also possible to apply the complex description of signals to band-limited noise waveforms. We define $N(t)$ as the complex envelope of a narrow-band noise waveform $n(t)$. Thus

$$n(t) = R_\ell \{N(t) \, e^{j\Omega t}\}$$

as before and

$$N(t) = X_n(t) + j \, Y_n(t) \qquad (2.21)$$

defined the in-phase and quadrature components of the noise. Clearly, these two components of the noise may be obtained by sine and cosine multiplication of $n(t)$, followed by filtering, exactly as before.

Letting $\Phi(\omega)$ represent the power spectrum associated with $n(t)$, the autocorrelation function of the process is

$$\varphi(\tau) = \frac{1}{2\pi} \int_{-\infty}^{+\infty} \Phi(\omega) \, e^{j\omega\tau} \, d\omega \qquad (2.22)$$

The corresponding analytic function $c(t)$ is given in this case by

$$c(\tau) = \frac{1}{\pi} \int_{0}^{\infty} \Phi(\omega) \, e^{j\omega\tau} \, d\omega = c(\tau) \, e^{j\Omega\tau} \qquad (2.23)$$

A well-known[13] result of this is that for stationary narrow-band processes

$$\langle X_n(t_1) \, X_n(t_2) \rangle = \langle Y_n(t_1) \, Y_n(t_2) \rangle = R_\ell\{C(t_1 - t_2)\}$$

$$\qquad (2.24)$$

$$\langle Y_n(t_1) \, X_n(t_2) \rangle = \langle X_n(t_1) \, Y_n(t_2) \rangle = I_m\{C(t_1 - t_2)\}$$

$C(t_1 - t_2)$ is the complex envelope of $C(\tau)$. We shall make use of two consequences of this result:

    1. If the noise is a Gaussian process, the $X_n(t)$ and $Y_n(t)$ are also Gaussian since they are the results of linear operations on Gaussian random variables.

    2. Since $\Phi(\omega)$ must be real, $C(\tau)$ must be of the form

$$C(\tau) = \{E(\tau) + j \, O(\tau)\} \, e^{j\omega_c \tau} \qquad (2.25)$$

where $E(\tau)$ and $O(\tau)$ represent even and odd functions respectively. If, in addition, $\Phi(\omega' t \, \Omega)$ is even about the ω' origin (perhaps requiring a suitable choice of Ω), then in addition $O(\tau) = 0$. $C(\tau) = E(\tau) + j(0)$ and thus, $X_n(t)$ and $Y_n(t)$ are statistically independent from Eqs. 2.24.

B. THE SCATTERING PROCESS

If we now consider the fields in a common reference frame originating from an oscillator at frequency Ω, the Maxwell equations in homogeneous media are

$$\nabla \times \overline{E} = -j\Omega\mu\overline{H}$$

$$\nabla \times \overline{H} = j\Omega\epsilon\overline{E} + \overline{J}$$

$$\nabla \cdot \overline{H} = 0 \tag{2.26}$$

$$\nabla \cdot \overline{E} = \rho/\epsilon$$

We have used our complex representation to write vectors as $\overline{V} e^{j\Omega t}$.

Any divergenceless vector is the curl of some other vector, so

$$\overline{H} = \nabla \times \overline{A} \tag{2.27}$$

Substituting the above into Eqs. 2.26, we have

$$\nabla \times (\overline{E} + j\Omega\overline{A}) = 0 \tag{2.28}$$

where $\overline{A}$ is the magnetic vector potential.

Now, invoking the complementary relationship that a curl-free vector is the gradient of some scalar gives

$$\overline{E} + j\Omega\overline{A} = -\nabla\phi$$

or
$$\overline{E} = -\nabla\phi - j\Omega\overline{A} \tag{2.29}$$

The function ϕ is the electric scalar potential.

Choosing $\nabla \cdot \overline{A} = -j\Omega\epsilon\phi$, so that $\overline{A}$ corresponds to a Lorentz gauge,

$$\overline{E} = -j\Omega\overline{A} + \frac{1}{j\Omega\epsilon} \nabla(\nabla \cdot \overline{A})$$

and   (2.30)

$$H = \nabla \times \overline{A}$$

We shall use the expression for $\overline{A}$ in terms of the volume current distribution $\overline{J}(\overline{r})$.

$$\overline{A}(\overline{r}) = \frac{\mu}{4\pi} \int_{V'} \frac{\overline{J}(\overline{r}') \, e^{-jk|\overline{r}-\overline{r}'|}}{|\overline{r}-\overline{r}'|} \, dv'$$ (2.31)

Here, $\overline{r}$ and $\overline{r}'$ are position vectors used to denote field points and source points, respectively, and to emphasize that the $\overline{A}$, to be evaluated at $\overline{r}$, results from $\overline{J}(\overline{r}')$ integrated over V'. As usual k is the magnitude of the wave vector

$$k = |\overline{k}| = \frac{2\pi}{\lambda}$$
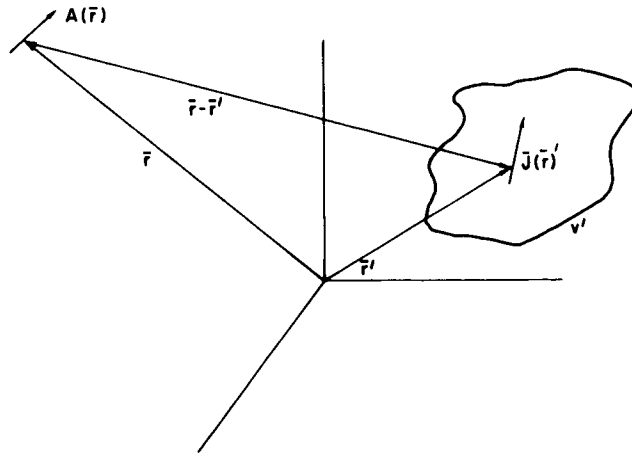
A general illustration is given in Fig. 2.

FIG. 2.   GEOMETRY FOR EQ. 2.31.

Reintroducing the $e^{j\Omega t}$,

$$\overline{A}(\overline{r}) \, e^{j\Omega t} = e^{j\Omega t} \frac{\mu}{4\pi} \int_{V'} \frac{\overline{J}(\overline{r}') \, e^{-jk|\overline{r}-\overline{r}'|}}{|\overline{r}-\overline{r}'|} \, dv' \qquad (2.32)$$

we see that $\overline{A}(\overline{r})$ is the complex envelope associated with out representation of the magnetic vector potential. Although at the moment $\overline{A}$ is a constant in time, it will not remain so. The electric field will be determined from Eq. 2.30 by substituting the representation of 2.31 for the vector potential.

Calculating $\nabla_{\overline{r}} \cdot \overline{A}(\overline{r})$

$$\nabla_{\overline{r}} \cdot \overline{A}(\overline{r}) = \frac{\mu}{4\pi} \nabla_{\overline{r}} \cdot \int_{V'} \frac{\overline{J}(\overline{r}') \, e^{-jk|\overline{r}-\overline{r}'|}}{|\overline{r}-\overline{r}'|} \, dv' \qquad (2.33)$$

$$= \frac{-jk\mu}{4\pi} \int_{V'} \frac{\overline{J}(r') \cdot \overline{u}_{\overline{r}\overline{r}'} \, e^{-jk|\overline{r}-\overline{r}'|}}{|\overline{r}-\overline{r}'|} \, dv'$$

$$- \frac{\mu}{4\pi} \int_{V'} \frac{\overline{J}(\overline{r}') \cdot \overline{u}_{\overline{r}\overline{r}'} \, e^{-jk|r-r'|}}{|\overline{r}-\overline{r}'|^2} \, dv' \qquad (2.34)$$

$$\overline{u}_{\overline{r}\overline{r}'} = \frac{\overline{r}-\overline{r}'}{|\overline{r}-\overline{r}'|}$$

By restricting ourselves to $\overline{r}$ far removed from V', the second term may be neglected with respect to the first. Taking $\nabla_{\overline{r}}(\nabla_{\overline{r}} \cdot \overline{A})$ gives

$$\nabla_{\overline{r}}(\nabla_{\overline{r}} \cdot \overline{A}) = - \frac{k^2 \mu}{4\pi} \int_{V'} \frac{(\overline{J}(\overline{r}') \cdot \overline{u}_{\overline{r}\overline{r}'})\overline{u}_{\overline{r}\overline{r}'} \, e^{-jk|\overline{r}-\overline{r}'|}}{|\overline{r}-\overline{r}'|} \, dv'$$

$$+ jk \frac{\mu}{4\pi} \int_{V'} \frac{(\overline{J}(\overline{r}') \cdot \overline{u}_{\overline{r}\overline{r}'})\overline{u}_{\overline{r}\overline{r}} \, e^{-jk|\overline{r}-\overline{r}'|}}{|\overline{r}-\overline{r}'|^2} \, dv' \qquad (2.35)$$

15

Dropping the term in $1/|\bar{r}-\bar{r}'|^2$ again and substituting in Eq. 2.30

$$E(\bar{r}) = -j\frac{\Omega\mu}{4\pi}\int_{V'}\frac{\bar{J}(\bar{r}')\ e^{-jk|\bar{r}-\bar{r}'|}}{|\bar{r}-\bar{r}'|}\ dv' + j\frac{\Omega\mu}{4\pi}\int_{V'}\frac{(\bar{J}(\bar{r}')\cdot\bar{u}_{rr'})\bar{u}_{rr'}e^{-jk|r-r'|}}{|\bar{r}-\bar{r}'|}\ dv'$$

$$= -j\frac{\Omega\mu}{4\pi}\int_{V'}\frac{(\bar{J}(\bar{r}')\cdot\bar{u}_{rr'})\bar{u}_{rr'} - \bar{J}(\bar{r}')\ e^{-jk|\bar{r}-\bar{r}'|}}{|\bar{r}-\bar{r}'|}\ dv' \qquad (2.36)$$

The bracketed terms in the integral are the components of $\bar{J}(\bar{r}')$ normal to the direction of propagation. This will be denoted by

$$\bar{J}_n(\bar{r}') = (\bar{J}(r')\cdot\bar{u}_{rr'})\ \bar{u}_{rr'} - \bar{J}(\bar{r}') \qquad (2.37)$$

By ignoring the higher order terms in the demoninator and assuming $\bar{r}$ far removed from the volume V' we have restricted ourselves to the radiation fields. Except when explicitly noted this will be the case from now on.

Equation 2.36 illustrates an important property of electromagnetic radiation; i.e., except for a constant, the radiated fields in any direction may be considered as a linear superposition of the currents that produced them, retarded in phase by $k|\bar{r}-\bar{r}'|$, and attenuated by $1/|r-r'|$. In particular, $\bar{E}(\bar{r})$ results from the convolution of a point radiation source, $e^{-jk|\bar{r}|}/|\bar{r}|$ and the function $\bar{J}_n(\bar{r}')$. Furthermore, the only physically restrictive assumption about the nature of $\bar{J}_n(\bar{r}')$ is that it exists in electrically homogeneous and unbound media.

These results apply almost automatically to the radiation from planetary surfaces. The volume over which our currents exist becomes a thin region containing the part of the planet in which we are interested, while the currents themselves tend to sheets. For the surface of a planet we might have a situation similar to that given in Fig. 3. Thus we write

$$\bar{A}(\bar{r}) = \frac{\mu}{4\pi}\int_{s'}\frac{\bar{K}(\bar{r}')\ e^{-jk|\bar{r}-\bar{r}'|}}{|\bar{r}-\bar{r}'|}\ ds' \qquad (2.38)$$
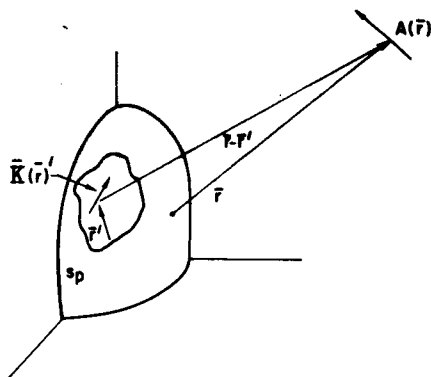
FIG. 3. GEOMETRY FOR EQ. 2.38.

when S' = the surface of integration and $\overline{K}(\overline{r}')$ = current sheet on s: We do this with the understanding that $\overline{K}(\overline{r}')$ may in fact have depth, and that if it does, we must take it into account by reverting to integrals over volumes.

In more complicated situations, where the fields can no longer be considered monochromatic, it is possible to extend the formulation that we have outlined directly via the Fourier transform.[14,15] However, that will not be necessary here.

To use these relations in the problem at hand, we adopt the view that the currents in our integrals are the result of incident radiation from a distant source impinging upon our surface. The reradiated, or scattered waves, are then given by Eqs. 2.37, 2.38. Unfortunately, the relationship between these currents and the source fields producing them is one of the most difficult problems in electromagnetic theory, and one in which little progress has been made. Fortunately for us, however, the form of the scattered wave given is sufficient for our work. The important property of the scattering, and the one that is critical to the later developments in this study, is that no matter what the surface is like, or how the surface currents are generated, the radiation fields can always be considered as arising from a continuous distribution of point sources.

C. THE POLAR SCATTERING DIAGRAM AND BRIGHTNESS DISTRIBUTION

Most radar measurements ultimately consist of a determination of the power scattered into the receiver by the target for some particular

set of antenna and receiver parameters. The quantities of interest might be the signal level present on an absolute scale, the ratio of the transmitted-to-received signal, or both the absolute and relative values. Consequently, it is necessary to have a parameter that describes the target in terms of a power measurement by the radar. Such a parameter obviously serves two purposes. The first of these is to provide a standard for comparing different radar systems. The second, which is particularly applicable to radar as a scientific probe, is to characterize the target itself. The quantity apropos this usage is the target radar cross-section, which is defined as the capture area required to intercept exactly that amount of power from the transmitter, so that if it were to be isotropically reradiated, it would scatter the same power into the receiver as does the actual target. Using this definition, the radar equation is commonly written as

$$P_R = \frac{P_T G_T}{4\pi R_1^2} \cdot \frac{\sigma}{4\pi R_2^2} \cdot A_R \qquad (2.39)$$

where P_T and P_R are the transmitted and received powers; R_1 and R_2 are the ranges from the transmitter to the target and the target to the receiver, respectively; A_R is the effective area of the receiving antenna viewed from the target while G_T is the gain of the transmitting antenna in the target direction; σ is the radar cross-section that we have just defined. A sketch showing these quantities is given in Fig. 4.

When the target is very large compared with the other dimensions involved as in Fig. 5, the usage must be modified slightly. Since in this case it is usually possible to distinguish one part of the target surface from another, a differential radar cross-section is introduced. Thus, we have

$$\sigma^o = \frac{\Delta\sigma}{\Delta s} \qquad (2.40)$$
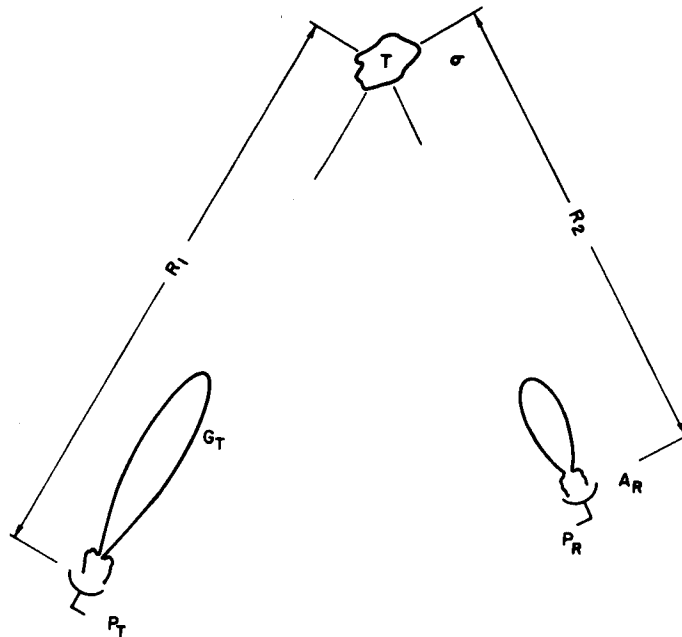
FIG. 4. ILLUSTRATING THE RADAR EQUATION.

where σ^o is the number of square meters of radar cross-section per unit area of target surface. The radar equation becomes

$$\Delta P_R = \frac{P_T G_T A_R \sigma^o}{(4\pi)^2 R_1^2 R_2^2} \cdot \Delta s \qquad (2.41)$$
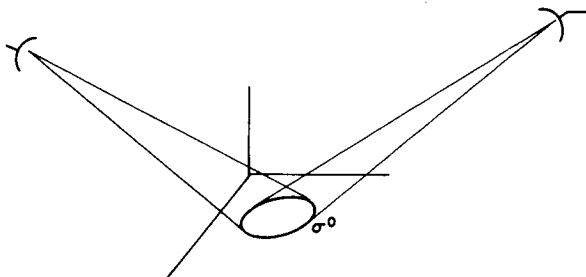
FIG. 5. RADAR CLOSE TO A SURFACE.

The term ΔP_R is the power scattered by the differential element Δs. σ^o has immediate expression as a ratio of the scattered and incident fields introduced in the previous section:

$$\sigma^0 = \frac{|E_s|^2}{|E_i|^2} \frac{4\pi R_2^2}{\Delta S} \tag{2.42}$$

It is clear from even the most cursory examination of Eqs. 2.37 and 2.38 that σ^0 is, in general, a function of both the direction of incidence and the direction of reflection. Introducing the polar angles of Fig. 6, θ_i, θ_r, θ_p as the angle of incidence, the angle of reflection, and the angle between the planes of incidence and the plane of reflection, respectively, allows explicit notation

$$\sigma^0 = \sigma^0(\theta_r, \theta_p; \theta_i) \tag{2.43}$$

The surface itself is assumed homogeneous in its scattering properties, so that σ^0 is independent of rotation about the normal from which θ_i and θ_r are measured.

FIG. 6. SCATTERING GEOMETRY.

The polar scattering diagram $\psi(\theta_r, \theta_p; \theta_i)$ is the normalized radar cross-section

$$\psi(\theta_r, \theta_p; \theta_i) = \frac{\sigma^0(\theta_r, \theta_p; \theta_i)}{\int_0^{2\pi} \int_0^{\pi/2} \sigma^0(\theta_r, \theta_p; \theta_i) \sin \theta_r \, d\theta_r \, d\theta_p} \tag{2.44}$$

shown in a manner completely analogous to the directivity of an antenna. Letting the total reflectivity be

$$\rho(\theta_i) = \int_0^{2\pi} \int_0^{\pi/2} \sigma^o(\theta_r, \theta_p; \theta_i) \sin \theta_r \, d\theta_r \, d\theta_p \qquad (2.45)$$

we write

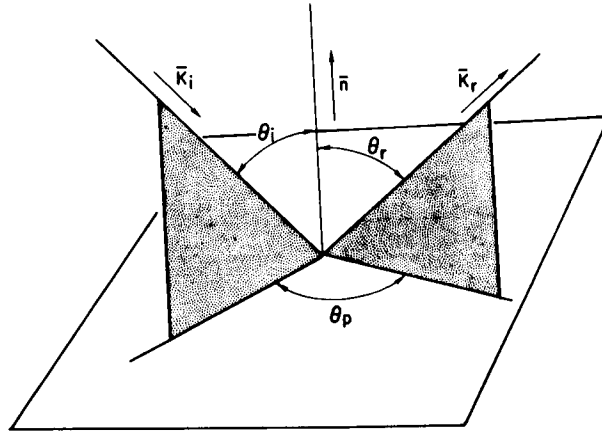$$\sigma^o = \rho(\theta_i) \, \Psi(\theta_r, \theta_p; \theta_i) \qquad (2.46)$$

Thus, a determination of $\sigma^o(\theta_r, \theta_p; \theta_i)$ is equivalent to a determination of the polar scattering diagram and a reflectivity factor $\rho(\theta_i)$.

While radar cross-section and the polar scattering diagram are extremely useful for describing the scattering from a single target or from an element of surface, they become awkward to use when expanded to include surfaces that exhibit considerable variation in their scattering properties from one point to another.

To escape these difficulties, we adopt another point of view. If we suppose for the moment that the surface is examined from some fixed vantage point, so that our angles of incidence and reflection are fixed for each portion of the surface, then we may introduce a brightness function $B(\bar{r})$, which depends only upon surface location. Using the standard definitions of total brightness[16] and σ^o as the differential radar cross-section at $\bar{r}$ for our particular angles of incidence and reflection, we have

$$B(\bar{r}; \theta_r, \theta_p, \theta_i) = \frac{P_T G_T}{4\pi R_1^2} \, \frac{\sigma^o(\bar{r}; \theta_r, \theta_p, \theta_i)}{4\pi} \qquad (2.47)$$

Assuming that the incident power per unit area of incoming wave is $1 w/m^2$ gives

$$\frac{P_R G_T}{4\pi R_1^2} = 1$$

SEL-67-042

and

$$B(\bar{r}; \; \theta_r, \; \theta_p, \; \theta_i) = \frac{\sigma^o(\bar{r}; \; \theta_r, \; \theta_p, \; \theta_i)}{4\pi} \qquad (2.48)$$

Thus, in effect, we have three names for the same thing. The brightness distribution $B(\bar{r})$, which we use when describing the power arriving from various portions of our surface; the polar scattering diagram Ψ, which we use when describing the angular dependence of the scatter of an elementary surface element; and the radar cross-section σ^o, which we use for convenience in the radar equation. Each of these has hidden in it the parameters and dependencies displayed by the other.

The albedo of a surface is the total brightness when integrated over the hemisphere above the surface for a given angle of incidence. From Eqs. 2.48 and Eq. 2.45, this is related to the reflectivity by

$$\text{Albedo} = 4\pi \; \rho(\theta_i) \; |E_i|^2 \; \left(\frac{\epsilon}{\mu}\right)^{1/2} \qquad (2.49)$$

Assuming $\bar{K}(\bar{r})$ is the result of E_i, the brightness may be easily related to the current distribution on the surface. Differentiating Eq. 2.38 with respect to s' we find

$$\Delta E = \frac{\Omega\mu}{4\pi} \frac{\bar{K}_n(\bar{r}') \; e^{-jk|\bar{r}-\bar{r}'|}}{|\bar{r}-\bar{r}'|} \qquad (2.50)$$

so that

$$\Delta P = |\Delta E|^2 \; \left(\frac{\epsilon}{\mu}\right)^{1/2} = \frac{\Omega^2(\epsilon\mu)^{1/2}}{(4\pi)^2} \frac{|\bar{K}_n(\bar{r}')|^2}{|\bar{r}-\bar{r}'|^2}$$

and

$$B(\bar{r}') \; \alpha \; |\bar{K}_n(\bar{r}')|^2 \qquad (2.51)$$

The brightness distribution is proportional to the magnitude squared of the current distribution on the surface.

D.   THE SCATTERED SIGNAL RECEIVED ON BOARD A SPACECRAFT

The developments of the preceding sections can now be used to de-rive some rather general properties of the radiation scattered by a planet. Having done so, it will be possible to predict the character-istics of the signals which will be seen by a bistatic-radar operating between the Earth and a spacecraft near the planet.

There are obviously two ways in which such a radar could operate. Either the transmitter remains on the ground while the receiver is carried into space, or the transmitter must become spaceborne while the receiver is left behind. Each of these two possibilities has its own advantages and disadvantages in practical terms. From a theoretical viewpoint, however, the reciprocity theorem assures us that they are equivalent, since the fields present at the receiver terminals must be the same in either case, all else being equal. But there are conceptual benefits to be gained from considering the first, or up-link, case where it is the receiver that is carried by the spacecraft; therefore, this is the case we will analyze.

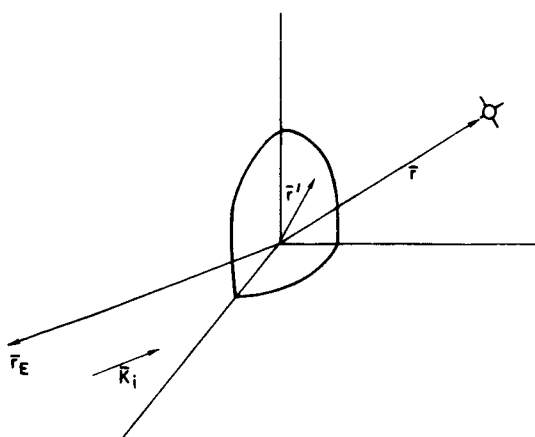

FIG. 7.   GEOMETRY FOR SCATTERING FROM PLANET.

Consider the situation depicted in Fig. 7. The origin of the coor-dinate system shown is at the center of the planet. In this system, $\bar{r}_E$, $\bar{r}'$ and $\bar{r}$ are position vectors of the Earth, a point of the sur-face of the planet, and the spacecraft, respectively. The planet is illuminated with radiation from the Earth of the form

$$E_i = E_o \, e^{j(\Omega t - \bar{k}_i \cdot \bar{r}_E)} \qquad (2.52)$$

As usual $\bar{k}_i$ is the incident wave vector in the direction of propagation. The Earth is assumed to be so remote that the magnitude of $\bar{E}_o$ is constant near the origin of our coordinate system. The resulting scattered wave is denoted $\bar{E}_s$ which, with the representation of Eq. 2.38, may be written as

$$\tilde{e}_s = \bar{E}_s \, e^{j\Omega t} = \frac{e^{j\Omega t} \mu}{4\pi} \int_{s'_p} \frac{\bar{K}(\bar{r}') \, e^{-jk|\bar{r}-\bar{r}'|} \, ds}{|\bar{r}-\bar{r}'|} \qquad (2.53)$$

As before, we need only concern ourselves with $\bar{E}_s$, the complex envelope of the analytic signal representation $\tilde{e}_s$. The area of integration s'_p is the surface included within the spacecraft horizon on the planet. The $e^{j\Omega t}$ comes directly from the assumption that the current and the scattered fields are caused by the e_i. The field distribution $\bar{E}_s$ is pictured as a fixed pattern attached to the planet in much the same way that an antenna pattern is associated with a physical antenna.

The spacecraft antenna pattern is taken into account by introducing an auxiliary coordinate system, parallel to the original and centered on the spacecraft as in Fig. 8. In the auxiliary system, let $g_v(\bar{u})$ denote the voltage gain pattern of the spacecraft antenna for a wave arriving from the $\bar{u}$ direction. Modifying the integral by weighting
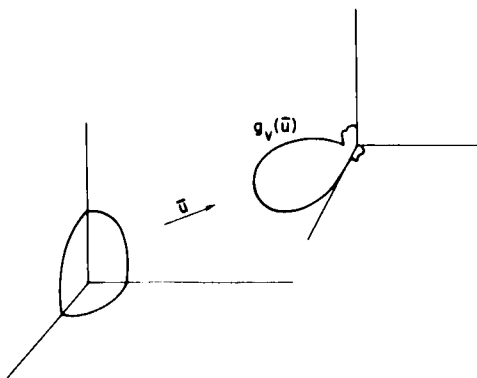

FIG. 8.   ANTENNA VOLTAGE GAIN.

each contribution to the field by the antenna gain in the direction from which it arrives, the voltage at the antenna terminals except for a constant is

$$\bar{V}(\bar{r}) = \int_{S'_p} \frac{\bar{K}(\bar{r}') \, e^{-jk|\bar{r}-\bar{r}'|}}{|\bar{r}-\bar{r}'|} \, g_r(\bar{u}_{\overline{rr}'}) \, ds \qquad (2.54)$$

Fjeldbo[4] has used an expansion similar to the method of stationary phase to analyze the case of scattering from a planet whose surface is generated by a zero mean, Gaussian random process superimposed upon a spherical surface. Starting from the Huygens-Khirchoff approximation and expanding about the point of specular reflection for the mean surface, Fjeldbo concluded that the average radar cross-section of a gently undulating planet is equal to that of a smooth sphere of equal size, and that the principal portion of the energy is returned from a region about the instantaneous specular point. The size of this region is determined by the probability, as one moves away from the specular point on the surface, of a plane tangent to the local surface being properly oriented to produce a reflection toward the spacecraft. In effect, his method selects the portions of the surface that tend to produce mirror-like reflections, in that the phases of the current distribution on these surfaces undergo a linear variation with $\bar{r}'$. Such surfaces are frequently thought of as plane facets or as gently curved surfaces which vary smoothly on the scale of a local Fresnel zone. Numerous other authors, while not applying their results to a spherical geometry for planets, have come to similar conclusions.

Contributions to the integral from regions where the phase is not stationary are not so easily handled. It is generally supposed that these regions correspond to portions of the surface that are extremely rough, or inhomogeneous, or vary in some other way that, on the scale of a wavelength, causes large phase fluctuations in our integral Eq. 2.53. The reradiation associated with these rapid phase fluctuations of the current sheet is called the diffuse component.

Generally, the fraction of the field generated by the diffuse component is much smaller than that from the quasi-specular. However, since the fields associated with these two mechanisms originate on different parts of the planet, they have different $\bar{u}_{\bar{r}\bar{r}'}$, and thus may be enhanced by a suitable choice of antenna function g_v. If the incident wave changes relative to the surface, as it must do when the planet rotates, a new pattern is generated. However, until the rotation is great enough to cause significant variations in the magnitude of the current distributions, the effect is to modify the phases of the current distribution by the change in the phase path of the illuminating wave. This may be displayed in our integral by factoring out the phase retardation of the incoming wave.

$$\bar{E}_s = \frac{\mu}{4\pi} \int_{s_p'} \frac{\bar{K}'(\bar{r}') \, e^{-j\bar{k}_i \cdot \bar{r}' - jk|\bar{r}-\bar{r}'|}}{|\bar{r}-\bar{r}'|} \, ds$$

$$(2.55)$$

$$\bar{K}'(\bar{r}') = \bar{K}(\bar{r}') \, e^{+j\bar{k}_i \cdot \bar{r}'}$$

Thus far, e_s has been treated as a point function observed at $\bar{r}$. But recognizing that a spacecraft must be in motion and that planets rotate, the two position vectors $\bar{r}'$ and $\bar{r}$ must now be considered as functions of time. Writing this out:

$$\bar{E}_s(\bar{r}(t)) = \frac{\mu}{4\pi} \int_{s_p} \frac{\bar{K}'([r'(t)]) \, e^{-jk|\bar{r}(t)-[\bar{r}'(t)]| - j\bar{k}_i \cdot [\bar{r}'(t)]}}{|\bar{r}'(t) - [\bar{r}'(t)]|} \, ds$$

$$(2.56)$$

where $[\bar{r}(t)]$ is the retarded quantity $\bar{r}'\left(t - \frac{|\bar{r}-[\bar{r}']|}{c}\right)$. The phase from any point on the surface is

$$\varphi(t) = -\bar{k}_i \cdot [\bar{r}'(t)] - k\bar{u}_{\bar{r}\bar{r}'}(t) \cdot (\bar{r}(t) - [\bar{r}'(t)]) \qquad (2.57)$$

The unit vector $\bar{u}_{\bar{r}\bar{r}'}$, must now be defined in terms of $\bar{r}$, and the retarded $\bar{r}'$. Frequency is the time derivative of phase. So

$$\omega(t) = \frac{d}{dt}\varphi(t) = -\bar{k}_i \cdot [\dot{\bar{r}}'] - \bar{k}_{\bar{r}\bar{r}'} \cdot (\dot{\bar{r}} - [\dot{\bar{r}}']) \qquad (2.58)$$

This is simply the expression for the Doppler shift associated with the relative motion of the points $\bar{r}$ and $\bar{r}'$. The total scattered signal is the composite of many small signals of different frequencies. It is clear from Eq. 2.58 that $\bar{E}_s(t)$ is band-limited, since all the terms on the right are finite. Furthermore, it is also easy to show that $\bar{E}_s(\bar{r}(t))$ represents a narrow-band signal for all spacecraft velocities much less than the speed of light. Thus, we see that the effect of spacecraft motion is to map points on the planet into the instantaneous frequency domain by the scalar product of the velocity vector and the wave vector. This mapping is not necessarily one-to-one, since several points may share the same instantaneous Doppler frequency. However, it should be clear that points close together on the surface must remain close in frequency. Bright spots on the surface will show up a strong component of the frequency spectrum of the scattered signal.

It is also convenient to be able to describe the variation of the scattered fields without reference to time. For this we use path length along the trajectory as a coordinate with the vector relations

$$\bar{s}(t) = \int_{t_o}^{t} \bar{v}(t)\, dt \qquad (2.59)$$

and

$$\dot{\bar{s}}(t) = \bar{v}(t) = \frac{d\bar{s}}{dt}$$

Distance measured along the path will be called ζ. We define the spatial frequency in the direction $\bar{u}$ as

$$\hat{\omega} = \nabla\varphi \cdot \bar{u} \qquad (2.60)$$

This is easily related to the Doppler frequency by $|\bar{v}|$

$$\omega = (\nabla\varphi \cdot \bar{u})|\bar{v}| = \omega|\bar{v}| \tag{2.61}$$

For a spacecraft less than a few planetary radii from the surface, the velocity of the vehicle is a great deal higher than that of a point on the surface,

$$\dot{\bar{r}}' \ll \dot{\bar{r}}$$

so that the Doppler shift is dominated by the spacecraft velocity

$$\omega \doteq \bar{k}_{rr'} \cdot \bar{u}_v$$

where

$$\bar{u}_v = \dot{\bar{r}}/|\bar{v}|$$

With this approximation, the spatial frequency is just the projection of the wave vector $\bar{k}_{rr'}$ onto the spacecraft trajectory.

The same considerations apply to the incident wave at the spacecraft

$$E_i = E_0 \, e^{-j\bar{k}_i \cdot \bar{r}} \tag{2.62}$$

$$\omega = \bar{k}_i \cdot \bar{v}$$

$$\hat{\omega} = \bar{k}_i \cdot \bar{u}_v \tag{2.63}$$

The signal present at the spacecraft is the narrow-band composite of the scattered signals from the entire surface visible from $\bar{r}$, with each component shifted in frequency by its direction of arrival and weighted in amplitude by the root modulus brightness of the surface and the antenna gain toward it. Viewed from the spacecraft, the brightest region will be the portion of the planet around the specular reflection.

In addition, the incident wave is also present at the spacecraft with the standard Doppler shift.

It should also be noted that beamwidth, as applied to an antenna, and bandwidth, as applied to a filter in the frequency domain, are virtually synonymous in this case. The only restriction is that we think of beamwidth in a plane containing the velocity vector. Since the antenna gain, $g_v(\bar{u})$, is a function of $\bar{u}$ alone, and the Doppler frequency for an arbitrary direction is essentially a function of the same vector variable $\bar{u}$, as $k(\bar{u} \cdot \bar{v})$, it is impossible to have frequencies present from targets outside the beam. Conversely, if the input to the spacecraft receiver is preceded by a narrow-band filter, it is impossible to have signals present from directions such that ω lies outside of the receiver passband.

III. <u>INVERSION OF DISCRETE SCATTERERS</u>

A. HEURISTIC DEVELOPMENT

In the preceding chapter, we considered the total signal scattered from a planet and related this signal to the current distribution on the surface. We also found that the magnitude squared of the currents is directly related to surface brightness in both an intuitive and rigorous sense. Our purpose now is to seek methods of recovering the brightness distribution from a measurement of the scattered fields.

To begin, it is instructive to adopt the standard radar problem approach and to consider the radiation from a single point on the planet's surface and the means by which this point might be distinguished from all others. This is accomplished by substituting a point source for $K(\bar{r}')$ in Eq. 2.38 of the preceding chapter. Since each component of the electromagnetic fields propagates in exactly the same way, the vector notation for the scattered wave will be dropped. The following equations will thus apply to each component of the fields individually and, if necessary, the vector fields can always be reconstructed.

Using two-dimensional Dirac delta function of strength a

$$K(\bar{r}') = a\, \delta(\bar{r}' - \bar{p}) \qquad (3.1)$$

$$E_s = \frac{a\, e^{-j\bar{k}_i \cdot \bar{p} - j\bar{k}_{pr} \cdot (\bar{r}-\bar{p})}}{|\bar{r}-\bar{p}|} \qquad (3.2)$$

or using the notation of Chapter II

$$\varphi = -\bar{k}_i \cdot \bar{p} - \bar{k}_{pr} \cdot (\bar{r}-\bar{p}) \qquad (3.3)$$

$$E_s = \frac{a\, e^{j\varphi}}{|\bar{r}-\bar{p}|} \qquad (3.4)$$

The geometry is the same as that given in Fig. 7, with $\bar{r}'$ replaced by $\bar{p}$. As a function of time, t, or of the spatial variable s along the path, this fits neatly into a line in cylindrical coordinates, such as the one illustrated in Fig. 9.
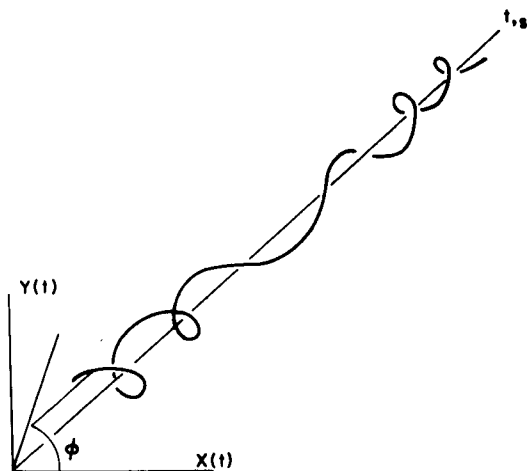
FIG. 9. COMPLEX ENVELOPE OF SIGNAL FROM POINT TARGET.

Here, we have depicted the trajectory of the complex envelope signal, as the spacecraft approached and moved past our target. Frequency deviation from the carrier is given by the tightness of the winding with the sign of frequency deviation determined by its sense, i.e., right or left. Amplitude is indicated by the diameter of the coil. There is an initial increase in phase due to the shortening of the path as the spacecraft approaches, followed by a stationary point at the moment of closest approach, and finally by an unwinding of the coil as the spacecraft recedes.

Suppose that we consider another point $\bar{p}'$, which is different from $\bar{p}$. Then, as before, we have

$$K(r') = a' \; \delta(\bar{r}' - \bar{p}') \tag{3.5}$$

and

$$E_s' = \frac{a' \; e^{j\varphi'}}{|\bar{r} - \bar{p}'|} \tag{3.6}$$

This second primed signal is similar in every respect to the first, and Fig. 9 represents E_s' as well as it does E_s. However, the difference in their phase functions, φ and φ', provides an important distinction. If, for example, the spacecraft passes the unprimed target before the primed, then the signal from the first is rapidly unwinding at the stationary point of the second. If the spacecraft passes both targets at the same instant so that the stationary points occur together, then either the targets are at the same distance from the spacecraft or they are not. If they are not at the same distance, then the signals must wind and unwind at different rates since $(\dot{\bar{r}} - \dot{\bar{p}}) \neq (\dot{\bar{r}} - \dot{\bar{p}}')$ for any point other than the stationary point. Furthermore, these characteristics of the phases are independent of the amplitudes

A method for separating these two signals, i.e., recovering the amplitudes of the currents at $\bar{p}$ and $\bar{p}'$, suggests itself. Through the linearity of the scattering process, the composite signal from $\bar{p}$ and $\bar{p}'$ is the sum of the contribution from each.

$$E = \frac{a\ e^{j\varphi}}{|\bar{r}-\bar{p}|} + \frac{a'\ e^{j\varphi'}}{|\bar{r}-\bar{p}'|} \tag{3.7}$$

Therefore, if we can unwind E by the amount corresponding to the phase of either E_s or E_s', the result will be a complex constant plus a term that fluctuates with the difference in phase of the primed and unprimed signals. Mathematically, this corresponds to multiplication by $e^{-j\varphi}$ or $e^{-j\varphi'}$ with the result that

$$e^{-j\varphi}\ E = \frac{a}{|\bar{r}-\bar{p}|} + \frac{a'\ e^{-j\psi}}{|\bar{r}-\bar{p}'|} \tag{3.8}$$

or

$$e^{-j\varphi'}\ E = \frac{a\ e^{j\psi}}{|\bar{r}-\bar{p}|} + \frac{a'}{|\bar{r}-\bar{p}'|} \tag{3.9}$$

where

$$\psi = \varphi - \varphi' \qquad\qquad (3.10)$$

Integration over many fluctuations of $e^{\pm j\psi}$ should then reduce the unwanted terms to a small fraction of the total. For example, from Eq. 3.8 we would expect

$$\int_{s_0}^{s_1} e^{-j\varphi}\, E d\ell = a \int_{s_0}^{s_1} \frac{d\ell}{|\bar{r}-\bar{p}|} + a' \int_{s_0}^{s_1} \frac{e^{-j\psi}}{|\bar{r}-\bar{p}'|}\, d\ell$$

$$\simeq a\, \frac{(s_1-s_0)}{|\bar{r}-\bar{p}|} + \text{small terms if} \quad |\bar{r}-\bar{p}| \qquad (3.11)$$
$$\text{variations are slight.}$$

The corresponding block diagram is given below in Fig. 10.
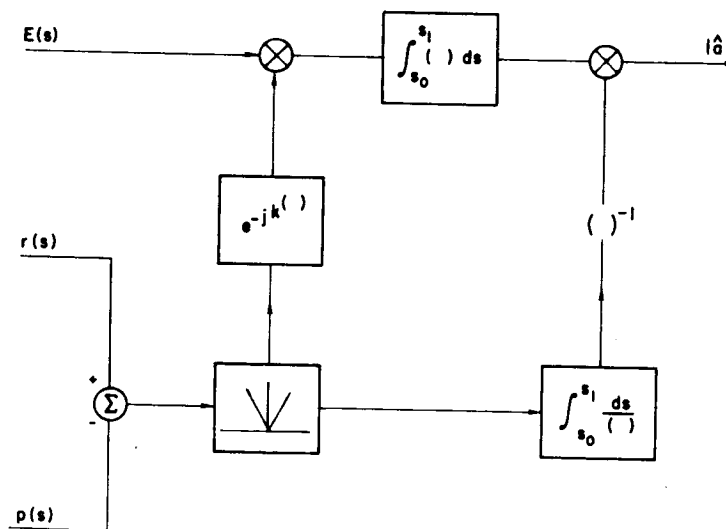
FIG. 10. DIAGRAM FOR PROCESSING SIGNAL FROM
TARGET AT $\bar{p}$.

From this, we may immediately generalize that for a set of discrete scatters

SEL-67-042

$$E = \sum \frac{a_i \, e^{j\varphi_i}}{|\bar{r}-\bar{p}_i|} \qquad (3.12)$$

and

$$\psi_{ik} = \varphi_i - \varphi_k \qquad (3.13)$$

To recover

$$\int_{s_0}^{s_1} e^{-j\varphi m} \, E d\ell = a_m \int_{s_0}^{s_1} \frac{d\ell}{|\bar{r}-\bar{p}_m|} + \sum_{i \neq m} \int_{s_0}^{s_1} \frac{a_i \, e^{j\psi im} \, d\ell}{|\bar{r}-\bar{p}_i|}$$

$$= am \, \frac{(s_1 - s_0)}{|\bar{r}-\bar{p}_m|} + \sum \text{ (small terms)} \qquad (3.14)$$

These operations are possible because of our assumed knowledge of the spacecraft trajectory.

A block diagram for these operations is given below in Fig. 11.

FIG. 11. PARALLEL PROCESSOR FOR MANY POINTS.

It should always be borne in mind that E represents data, a measurement of the scattered wave, over some portion of the spacecraft trajectory.

B. THE RESOLUTION CELL

The ultimate usefulness of an image lies in the finest detail that it preserves, or, in turn, upon the minimum distance that can exist between 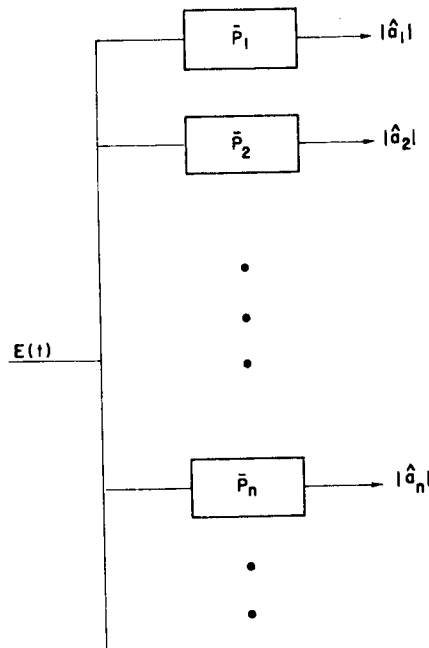two points and still allow them to be distinguished from one another. The classical optical function used for this purpose is the spatial distribution in the image space of the field intensity corresponding to an optical point source, or the image point response.

A similar approach is applied to the monostatic radar problem, in that it is the radar system's power response to a point target that is taken as a measure of the system's capability to resolve closely spaced targets. Instead of an optical system with an image plane, we now have a receiver processing the returning signals in time-frequency space to determine target range and velocity. The resolution that may be obtained is directly related to the waveform used, and is characterized by the ambiguity function. Unfortunately, the ambiguity function does not apply here for two reasons: (1) we are interested in a resolution cell on the surface of our planet rather than in time-frequency, and (2) the signal arriving from each of our scatterers is a different function rather than a standard signal with a continuum of time-frequency displacements, as required by the assumptions in the development of the ambiguity function.

However, the physical basis for calculating the point response is the same for both the radar and optical problems. That basis is the assumption that the absolute phases of all parts of the target are statistically independent, so that on the average, it is the powers, or intensities, of the responses from each target point that will be superimposed in the image. This same assumption will be made here, but a hybrid approach is taken to the calculation. The signal is considered as processed in a manner similar to that described in Section A above. But, for purposes of analysis, it is associated with the geometry that existed when the signal was received. With this approach, our problem becomes somewhat geometrical.

The points $\bar{p}$ and $\bar{p}'$ and a fraction of the spacecraft's trajectory are shown in Fig. 12. For the purpose of this computation, the trajectory is assumed to be linear.
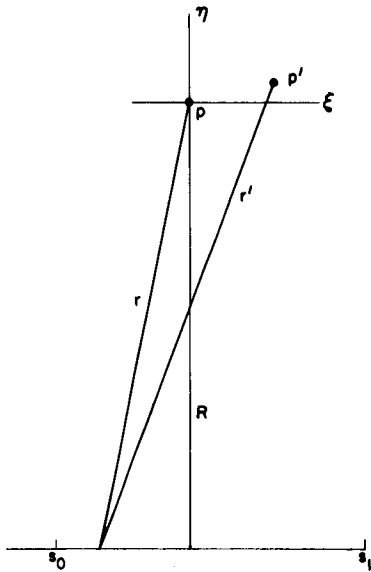
FIG. 12. RELATION OF $\bar{p}$ AND $\bar{p}'$.

A coordinate system is centered on the point p as shown. For convenience p, p' and the trajectory are also assumed to be co-planar. The functions r and r' are the distances to $\bar{p}$ and $\bar{p}'$ from the point s respectively, while R is the distance of closest approach.

Any results obtained from the co-planar assumption may be applied to the planetary case by rotating points on the sphere about the trajectory until they lie in a common plane. Using our new variables, the analytic signal on s is

$$E(s) = \frac{a \; e^{j\varphi}}{r} + \frac{a' \; e^{j\varphi'}}{r'} \qquad (3.15)$$

$$\varphi = -kr \qquad (3.16)$$

$$\varphi' = -kr'$$

Applying the operations of Fig. 10, and taking the magnitude squared to obtain power

$$|\hat{a}|^2 = \left| a + a' \int_{s_o}^{s_1} \frac{e^{-j\psi}}{r'} \, ds \bigg/ \int_{s_0}^{s_1} \frac{ds}{r} \right|^2 \qquad (3.17)$$

Expanding Eq. 3.17

$$|\hat{a}|^2 = |a|^2 + |a'|^2 \left| \int_{s_0}^{s_1} \frac{e^{-j\psi}}{r'} ds \bigg/ \int_{s_0}^{s_1} \frac{ds}{r} \right|^2$$

$$+ 2R\ell \left\{ a \, a' \int_{s_0}^{s_1} \frac{e^{-j\psi}}{r'} ds \bigg/ \int_{s_0}^{s_1} \frac{ds}{r} \right\} \qquad (3.18)$$

The last term is taken equal to zero by the independent phases argument. Thus, we are left with

$$|\hat{a}|^2 = |a|^2 + |a'|^2 \left| \int_{s_0}^{s_1} \frac{e^{-j\psi}}{r'} ds \bigg/ \int_{s_0}^{s_1} \frac{ds}{r} \right|^2 \qquad (3.19)$$

where the integral factor describes the effects of the target at p' on our evaluation of the brightness at p. This factor is also precisely the image point response, since it is the expression one would obtain for the response at p', due to a source at p. Therefore, we are led to a calculation of

$$g(\xi,\eta) = \int_{s_0}^{s_1} \frac{e^{-j\psi}}{r'} \bigg/ \int_{s_0}^{s_1} \frac{ds}{r} \qquad (3.20)$$

Starting with the exponent

$$\psi = -k(r-r') \qquad (3.21)$$

$$r = (R^2 + s^2)^{\frac{1}{2}}$$

$$= R\left(1 + \frac{s^2}{2R^2}\right) \qquad \frac{s}{R} \ll 1 \qquad (3.22)$$

$$r' = \left[(R-\eta)^2 + (s-\xi)^2 \right]^{1/2}$$

$$= (R-\eta) \left[1 + \frac{(s-\xi)^2}{2(R-\eta)^2} \right] \quad \frac{s-\xi}{R-\eta} \ll 1 \qquad (3.23)$$

the difference between these two terms is

$$r-r' = \frac{s^2}{2R} - \frac{(s-\xi)^2}{2(R-\eta)} + \eta$$

$$= \frac{2R\xi s - s^2\eta + R\xi^2 + 2R\eta(R-\eta)}{2R(R-\eta)} \qquad (3.24)$$

When applied to the integral, the last two terms in Eq. 3.24 will give only a constant phase factor and may be dropped leaving

$$r-r' = \frac{-s^2\eta + 2Rs\xi}{2R(R-\eta)} \qquad (3.25)$$

as the important part of the path difference. Completing the square in Eq. 3.24 yields

$$\frac{-1}{2R(R-\eta)} \left\{ \left(\eta^{1/2}s - \eta^{-1/2}\xi R \right)^2 - \frac{\xi^2 R^2}{\eta} \right\}, \quad \eta \neq 0 \qquad (3.26)$$

and dropping the constant term again and substituting $2\pi/\lambda$ for k further reduces the exponent expression to

$$\psi(s) = \frac{-\pi/\lambda}{R(R-\eta)} \left(\eta^{1/2}s - \eta^{-1/2}\xi R \right)^2 \qquad (3.27)$$

Under the assumptions required for the binomial expansion approximation in the exponent, the variation in the denominator of the upper integral is also small and approximately equal to R. The lower integral may be evaluated in terms of the inverse tangent.

$$g(\xi, \eta) = \frac{1}{R \tan^{-1} s/R \Big|_{s_0}^{s_1}} \int_{s_0}^{s_1} e^{-j \frac{\pi/\lambda}{R(R-\eta)} (\eta^{1/2}s - \eta^{-1/2}\xi R)^2} ds \qquad (3.28)$$

letting

$$z(s) = \left(\frac{z}{\lambda R(R-\eta)}\right)^{1/2} (\eta^{1/2}s - \eta^{-1/2}\xi R) \qquad (3.29)$$

yields

$$g(\xi, \eta) = \frac{1}{R \tan^{-1} s/R \Big|_{s_0}^{s_1}} \left(\frac{\lambda R(R-\eta)}{2\eta}\right)^{1/2} \int_{z(s_0)}^{z(s_1)} e^{-j \frac{\pi}{2} z^2} dz \qquad (3.30)$$

If we now express $R \tan^{-1} s/R \Big|_{s_2}^{s_1}$ as approximately equal to $s_1 - s_0$, then

$$g(\xi, \eta) = \frac{\left(\frac{\lambda R(r-\eta)}{2\eta}\right)^{1/2}}{(s_1 - s_0)} \int_{z(s_0)}^{z(s_1)} \left(\cos \frac{\pi}{2} z^2 + j \sin \frac{\pi}{2} z^2\right) dz \qquad (3.31)$$

Thus

$$I(\xi, \eta) = |g(\xi, \eta)|^2 = \frac{\lambda R(R-\eta)}{2\eta(s_1 - s_0)^2} \left\{ \left(C(z) \Big|_{z(s_0)}^{z(s_1)}\right)^2 + \left(S(z) \Big|_{z(s_0)}^{z(s_1)}\right)^2 \right\}$$

$$(3.32)$$

where

$$S(z) = \int_0^z \sin \frac{\pi}{2} z^2 \, dz$$

and

$$C(z) = \int_0^z \cos \frac{\pi}{2} z^2 \, dz$$

are the Fresnel integrals for sine and cosine respectively.

The expressions may be evaluated on the ξ axis by returning to Eq. 3.25: substituting

$$\eta = 0 , \quad r-r' = \xi \, s/R \tag{3.33}$$

so

$$g(\xi,0) = \frac{1}{s_1 - s_0} \int_{s_0}^{s_1} e^{-j \frac{2\pi}{\lambda} \xi \, s/R} \, ds \tag{3.34}$$

Equation 3.34 may be interpreted as the Fourier transform of a single pulse starting from s_0 and lasting until s_1 so

$$g(\xi,0) = \text{sinc}\left(\xi/\lambda \cdot \frac{s_1 - s_0}{R} \right) \tag{3.35}$$

$$I(\xi,0) = \text{sinc}^2\left(\xi/\lambda \cdot \frac{s_1 - s_0}{R} \right) \tag{3.36}$$

A contour plot of $I(\xi,\eta)$ for $R = 10^6$, $s_1 = s_0 = 10^5$, is given in Fig. 13.
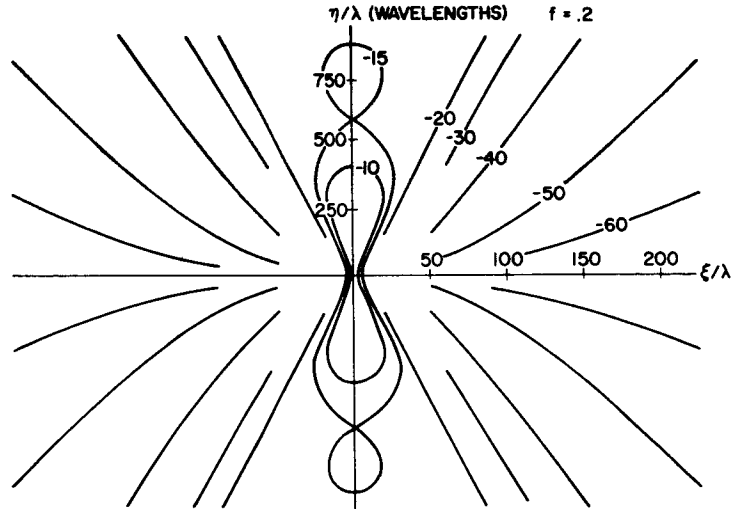
FIG. 13. ISOPHOTES OF POINT RESPONSE.

It is also useful to consider the on-axis resolution. For the η-axis, again substitute in Eq. 3.25, $\xi = 0$

$$r-r' = - \frac{s^2\eta}{2R(R-\eta)} \sim - \frac{s^2\eta}{2R^2} \quad \text{if} \quad R \gg \eta \qquad (3.37)$$

and

$$g(0,\eta) = \frac{1}{s_1 - s_0} \int_{s_0}^{s_1} e^{-j\frac{\pi}{\lambda}\frac{s^2\eta}{R^2}} \, ds \qquad (3.38)$$

letting $z = s/R$

$$g(0,\eta) = \frac{R}{(s_1 - s_0)} \int_{s_0/R}^{s_1/R} e^{-j\frac{\pi}{2}z^2 2\eta/\lambda} \, dz \qquad (3.39)$$

Taking the special case $s_1 = -s_0$ and $s_1/R = f/2$ provides considerable simplification

$$g(0,\eta) = \frac{2}{f} \int_0^{f/2} e^{-j\frac{\pi}{2}z^2\frac{2\eta}{\lambda}} \, dz \qquad (3.40)$$

Using the Fresnel integral again yields

$$I(0,\eta) = \frac{2\lambda}{f^2\eta}\left(C^2\left[f\left(\frac{\eta}{2\lambda}\right)^{\frac{1}{2}}\right] + S^2\left[f\left(\frac{\eta}{2\lambda}\right)\right]\right) \qquad (3.41)$$

It is a simple matter to show that this is well behaved at the origin and that $I(0,0) = 1$. The ξ-axis resolution may also be expressed in terms of the quantity f by substitution in Eq. 3.36:

$$I(\xi,0) = \text{sinc}^2(f\xi/\lambda) \qquad (3.42)$$

With these expressions, it is possible to evaluate the resolution in the ξ and η directions. A natural choice in the ξ direction is the distance between the first zeros of the sinc function. Thus:

$$\left(\Delta\xi/\lambda\right)f = 1$$

or

$$\Delta\xi/\lambda = \frac{1}{f} \qquad (3.43)$$

The choice is not quite so clear in the η direction since $I(0,\eta)$ has no zeros, and we take the value $I(0,\eta) = 0.1 \sim 1/\pi^2$ arbitrarily. Then using the asymptotic value of the Fresnel integrals

$$\left.\begin{array}{l}C(z) \rightarrow 1/2\\ S(z) \rightarrow 1/2\end{array}\right\} \quad \text{as} \quad z \rightarrow \infty$$

gives

$$I(0,\eta) = \frac{1}{\pi^2} = \frac{2}{f^2}\frac{\lambda}{\Delta\eta}\left[\left(\frac{1}{2}\right)^2 + \left(\frac{1}{2}\right)^2\right] = \frac{\lambda}{f^2\Delta\eta} \cdot \frac{1}{2}$$

or

$$\Delta\eta/\lambda \stackrel{\sim}{=} \frac{\pi^2}{2f^2} \qquad (3.44)$$

Doubling the result to account for both the η and $-\eta$ directions,

$$\frac{\Delta\eta}{\lambda} = \frac{\pi^2}{f^2} \qquad (3.45)$$

The resolution in the two dimensions ξ and η has been plotted in Fig. 14 from Eq. 3.43 and Eq. 3.44.
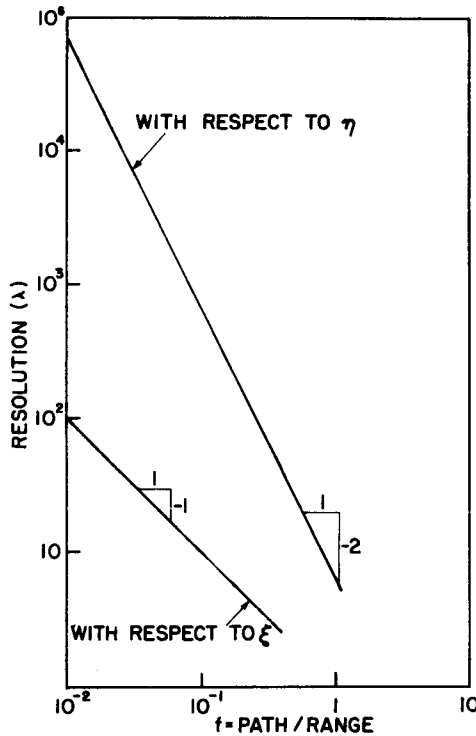
FIG. 14. RESOLUTION VS f NUMBER.

Obviously, the key to resolution in the η direction is to make f as large as possible. Note that so long as our approximations are satisfied, the results are independent of range.

A critical factor in the validity of the point response function $I(\xi,\eta)$ as an estimate of the resolution is its behavior for large ξ and η. If $I(\xi,\eta)$ does not fall off rapidly enough, then it is possible

for a collection of targets far removed from the origin of the ξ,η coordinate system to contribute a significant fraction of the total power when the data are processed to recover the signal from a particular p. The importance of this effect may be estimated by imagining that the contributing scatterers are uniformly distributed on the target surface, and by calculating the fraction of the total response that comes from a small area about the target point. Making the change of variables

$$\xi = \rho \cos \theta$$

$$\eta = \rho \sin \theta$$

(3.46)

the pertinent quantity becomes

$$\Lambda(\rho_o) = \frac{\int_0^{\rho_0} \int_0^{2\pi} I(\rho,\theta) \, \rho d\rho d\theta}{\int_0^{\infty} \int_0^{2\pi} I(\rho,\theta) \, \rho d\rho d\theta}$$

(3.47)

It does not seem possible to evaluate the integral from the expression for $I(\rho,\theta)$ which we already have, so we revert to the geometrical representation and begin again.
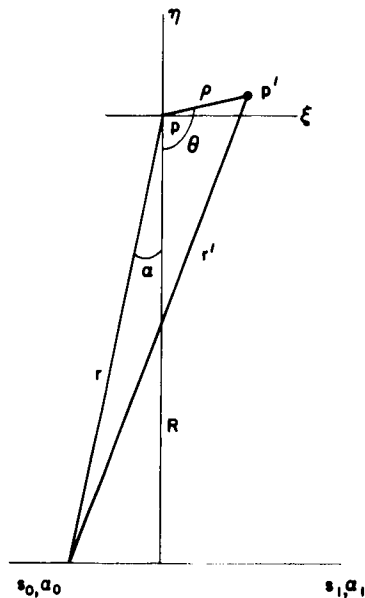

FIG. 15. GEOMETRY FOR CALCULATION OF $\Lambda(\rho)$.

From Fig. 15, the phase difference is

$$\psi \simeq \frac{2\pi}{\lambda} \cdot \rho \, \cos(\theta - \alpha) \qquad (3.48)$$

and the pertinent integral is

$$g(\rho, \theta) = \frac{1}{R} \int_{s_0}^{s_1} e^{-j\psi} \, ds = \int_{\alpha_0}^{\alpha_1} e^{-j\psi} \, d\alpha, \quad \alpha \doteq \frac{s}{R}$$

$$I(\rho, \theta) = g \cdot g^* = \int_{\alpha_0}^{\alpha_1} \int_{\alpha_0}^{\alpha_1} e^{-j(\psi(\alpha) - \psi(\alpha'))} \, d\alpha \, d\alpha' \qquad (3.49)$$

The integral over ρ, θ is

$$\int_0^{\rho_0} \int_0^{2\pi} I(\rho, \theta) \, \rho d\rho d\theta = \int_0^{\rho_0} \int_0^{2\pi} \int_{\alpha_0}^{\alpha_1} \int_{\alpha_0}^{\alpha_1} \rho e^{-j(\psi(\alpha) - \psi(\alpha'))} d\alpha d\alpha' d\rho d\theta$$

$$(3.50)$$

Now

$$\psi(\alpha) - \psi(\alpha') = \frac{2\pi}{\lambda} \rho [\cos(\theta - \alpha) - \cos(\theta - \alpha')] \qquad (3.51)$$

while

$$e^{jz \cos \theta} = J_0(z) + 2 \sum_{k=1}^{\infty} (-)^k J_{2k}(z) \cos(2 \, k \, \theta)$$

$$+ j \, 2 \sum_{k=1}^{\infty} (-)^k J_{2k+1} \sin[2(k+1)\theta] \qquad (3.52)$$

45

and therefore

$$e^{-j\frac{2\pi}{\lambda}\rho(\cos(\theta-\alpha) - \cos(\theta-\alpha'))} = e^{-j\frac{2\pi}{\lambda}\rho\cos(\theta-\alpha)} \cdot e^{+j\frac{2\pi}{\lambda}\rho\cos(\theta-\alpha')}$$

$$= J_0^2\left(\frac{2\pi}{\lambda}\rho\right) + \sum \text{ (sines and cosines products)} \qquad (3.53)$$

Integrating θ over 2π, an approximate bound is given by

$$\int_0^{\rho_0} \int_0^2 \rho I(\rho,\theta)\,d\rho d\theta < 2\pi \int_0^{\rho_0} \int_{\alpha_0}^{\alpha_1} \int_{\alpha_0}^{\alpha_1} \rho\, J_0^2\left(\frac{2\pi}{\lambda}\rho\right)\,d\rho\,d\alpha\,d\alpha'$$

$$= 2\pi(\alpha_1-\alpha_1)^2 \int_0^{\rho_0} \rho J_0\left(\frac{2\pi}{\lambda}\rho\right)\,d\rho \qquad (3.54)$$

The standard asymptotic form for $J_0(z)$ is

$$J_0(z) \rightarrow \left(\frac{2}{\pi z}\right)^{\frac{1}{2}} \sin z + 0|z|^{-1} \quad \text{as} \quad z \rightarrow \infty$$

$$J_0^2(z) \rightarrow \left(\frac{2}{\pi z}\right) \sin^2 z \qquad (3.55)$$

so that Eq. 3.54 is approximated by

$$\int_0^{\rho_0} \int_0^{2\pi} \rho I(\rho,\theta)\,d\rho d \leq \frac{\lambda}{\pi^2}(\alpha_1-\alpha_0)^2(\rho_0) \qquad (3.56)$$

For an infinite target plane the integrated response does not converge.

Equation 3.56 may be applied to a finite surface by placing an upper boundary on the integral in the denominator of ρ_{max}. Supposing that the target surface is made up of a set of discrete scatterers of average

power P and occupying area A, we have for the power from the total area included in ρ_{max}

$$\frac{\lambda}{\pi^2} (\alpha_1 - \alpha_0)^2 \rho_{max} (P/A) \qquad (3.57)$$

The power from a target at p is $P(\alpha_1 - \alpha_0)^2 / 2$ so that the ratio of the two is

$$\frac{(\text{Power from target})}{(\text{Power from total area})} = \frac{P(\alpha_1 - \alpha_0)^2 / 2}{\lambda \rho_{max} \dfrac{(\alpha_1 - \alpha_0)^2}{\pi^2} P/A}$$

$$= \frac{A\pi^2}{2\lambda \rho_{max}} \qquad (3.58)$$

Note that this result is independent of f number and hence independent of the length of the path over which the data are taken and of the shape of the resolution cell. The area of integration $\pi\rho_{max}^2$ may be limited either by the spacecraft antenna or the size of the planet itself.

C. THE EFFECT OF ERRORS ON THE INVERSION

In the last section, we considered the highly idealized case of an exact inversion with a linearized trajectory. By exact, we mean that our knowledge of the relative positions of the spacecraft and target is so complete that we can compute the φ_j without significant error. For the calculations made so far, we have, in effect, assumed knowledge of the spacecraft trajectory to a minute fraction of a wavelength. At best this is a highly unrealistic assumption. Furthermore, if high resolution is to be achieved, particularly in the dimension normal to the trajectory, it is necessary to have trajectory information over a path which is a significant decimal fraction of the range, R, to the target. In practical terms, this requires the collection of data over paths that cover

hundreds of thousands or even millions of wavelengths. Therefore, we consider the effects of errors on the reconstruction to determine the uncertainty that can be tolerated in the inversion.

The motion of a spacecraft is extremely smooth. In the two-body problem, where we need consider only radial accelerations, the derivatives of the spacecraft motion diminish rapidly with increasing order. Even when three bodies are concerned, as, for example, in the effect that a local moon or the Sun might have on a planetary orbiter, the effects of the third body are perturbations acting over periods of days or weeks. (cf. Ref. 17). Consequently, we need only consider the effects of an erroneous orbital determination. In other words, the errors in one calculation of the $\varphi_j(s)$ are due solely to an inaccurate determination in our theory of orbital motion. In Fig. 16, suppose that the true trajectory is s, but we think that it is s'.
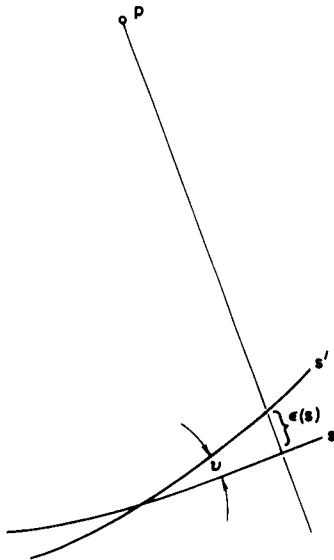

FIG. 16. DEFINING THE ERROR FUNCTION FOR THE SPACECRAFT TRAJECTORY.

If we process for the point at p, then we are in error by $\epsilon(s)$ rad/m and the point response function is

$$I_\epsilon(\xi, \eta) = \left| \int_{s_0}^{s_1} \frac{e^{-j(\psi+\epsilon)}}{r} \, ds \right|^2 R^2/(s_1 - s_0)^2 \qquad (3.59)$$

Using the previous approximations for $\psi(s)$

$$I_\epsilon(\xi,\eta) \propto \left| \int_{s_0}^{s_1} \frac{e^{-j \frac{\pi/\lambda(s^2\eta - 2R\,s)}{R(R-\eta)} + j\epsilon(s)}}{r} \, ds \right|^2 \qquad (3.60)$$

Supposing that the error is of the form

$$\epsilon(s) = as^2 + bs + c \qquad (3.61)$$

gives, from our expression for ψ,

$$\psi + \epsilon = -\frac{\pi}{\lambda} \left(\frac{\eta}{R(R-\eta)} - a \right) s^2$$

$$+ \left(\frac{\pi}{\lambda} \frac{2\xi}{R-\eta} + b \right) s + c \qquad (3.62)$$

Evidently, the result of errors up through the second order is to cause a shift in the response function by the amounts $\Delta\xi$, $\Delta\eta$

$$\Delta\xi = -\frac{\lambda}{\pi} \left(\frac{R-\eta}{2} \right) b$$

$$\Delta\eta = aR(R-\eta)\frac{\lambda}{\pi} \qquad (3.63)$$

That is, nothing is destroyed by errors of this type. The response function is preserved, but the signal we associate with p at the origin of the $\xi\eta$ coordinate system really belongs with $\Delta\xi$, $\Delta\eta$.

Considering only one term in $\epsilon(s)$ at a time reveals the physical significance of these terms. Denoting the angular error between s and s' by υ

$$b = \upsilon k = \upsilon\frac{2\pi}{\lambda} \qquad (3.64)$$

For small errors the displaced maxima will still be near the ξ, η origin and η will be small compared with the range, so that

$$\Delta\xi = \upsilon \frac{2\pi}{\lambda} \cdot \frac{\lambda}{2\pi} \cdot (R-\eta) \doteq \upsilon R \qquad (3.65)$$

Linear phase errors therefore shift the image point by angle υ.

For the second-order term alone, with the same approximation $R \gg \eta$, we have

$$\Delta\eta = -\frac{\lambda}{\pi} R^2 a \qquad (3.66)$$

so that the quadratic error translates directly into range. In terms of the radius of curvature of the orbit, R_o, it is a simple matter to show that

$$a = \left(\frac{1}{R_o^2} - \frac{1}{\left(R_o^2 + \Gamma\right)^2} \right) \frac{2\pi}{\lambda} \qquad (3.67)$$

where Γ is the error in our estimate of R_o. Thus

$$\Delta\eta = -2 \frac{R^2}{R_o^2} \left(1 - \frac{R_o^2}{(R_o + \Gamma)^2} \right) \qquad (3.68)$$

In general, one would expect errors from this source to be quite small.

The constant term makes no difference at all.

There is one other error of a sort similar to the ones we have just considered, and that is an error in the determination of the carrier frequency. In this case, the calculated phase paths that we use in our processor will all be in error by an amount proportional to the error in λ. If we let the true wavelength be λ_0 and the erroneous wavelength used in the processing be λ_ϵ, then, in the calculation of the point response, we must use

$$\psi = \frac{2\pi}{\lambda_o} r - \frac{2\pi}{\lambda_\epsilon} r'$$

$$\simeq \frac{2\pi}{\lambda_o}\left(R + \frac{s^2}{2R}\right) - \frac{2\pi}{\lambda_\epsilon}\left(R-\eta + \frac{(s-\xi)^2}{2(R-\eta)}\right) \qquad (3.69)$$

where we have again employed the approximation of Eqs. 3.22 and 23 and the geometry of Fig. 12.

Simplifying,

$$\psi = \frac{2\pi}{\lambda_o}\left\{R + \frac{s^2}{2R} - \frac{\lambda_o}{\lambda_\epsilon}\left(R-\eta + \frac{(s-\xi)^2}{2(R-\eta)}\right)\right\}$$

$$= \left\{R\left(1 - \frac{\lambda_o}{\lambda_\epsilon}\right) + \frac{s^2}{2R} - \frac{\lambda_o}{\lambda_\epsilon}\frac{(s-\xi)^2}{2(R-\eta)} + \frac{\lambda_o}{\lambda_\epsilon}\eta\right\} \cdot \qquad (3.70)$$

Again dropping the terms that are constant in s,

$$\psi \to \frac{2\pi}{\lambda_o}\left\{\frac{s^2(\lambda_o/\lambda_\epsilon)(R-\eta) - Rs^2 + 2R\xi s}{2R(R-\eta)\,\lambda_\epsilon/\lambda_o}\right\}$$

$$= \frac{2\pi}{\lambda_\epsilon}\left\{\frac{s^2\left[R\left(1 - \frac{\lambda_\epsilon}{\lambda_o}\right)-\eta\right] + 2R\xi s}{2R(R-\eta)}\right\} \qquad (3.71)$$

The principal effect is to shift change $I(\xi,\eta)$ to $I[\xi,\eta-R(1-\lambda_\epsilon/\lambda_o)]$.

The errors that we have considered thus far are peculiar, in that they produce systematic effects on our calculation. This is because they enter the calculation only once as the parameter of some function as, for example, in the use of an erroneous wavelength. A measurement error in the determination of the array of the conical elements that describe the path of an orbiter would be another. In this second case the mistake can be shown to propagate through the orbital computations to produce the linear and second-order effects that we have already discussed. We have seen that these errors have little or no practical

SEL-67-042

importance. However, the errors associated with the data itself may be critical. These may be imagined to arise in several ways, the most obvious of which include oscillator instabilities and sampling errors. More subtle difficulties would include the effects of any atmosphere through which our signals must pass and even the effects of the interplanetary medium on the propagation of the illuminating wave. It is supposed that all these sources of error will impose an additional random phase modulation on our data. The phase error function, $\epsilon(s)$, thus becomes a random variable, which is assumed to be stationary and ergodic. The error function may also be assumed to be zero mean without loss of generality since a constant may be added or subtracted from the phase without affecting our final results. Then, as before

$$g(\xi,\eta) \propto \int_{s_0}^{s_1} \frac{e^{-j(\psi+\epsilon)}}{r} \, ds \qquad (3.72)$$

and

$$\langle g(\xi,\eta) \rangle = \left\langle \int_{s_0}^{s_1} \frac{e^{-j(\psi+\epsilon)}}{r} \, ds \right\rangle = \int_{s_0}^{s_1} \frac{e^{-j\psi}}{r} \langle e^{-j\epsilon} \rangle \, ds \qquad (3.73)$$

where

$$\langle \quad \rangle = \int_{-\infty}^{+\infty} (\quad) \, p(\epsilon) d\epsilon$$

and $p(\epsilon)$ is the probability density function of the error function. Similarly,

$$\langle I(\xi,\eta) \rangle = \langle |g|^2 \rangle = \int_{s_0}^{s_1} \int_{s_0}^{s_1} \frac{e^{-j(\psi(s)-\psi(s'))}}{r^2} \left\langle e^{-j[\epsilon(s)-\epsilon(s')]} \right\rangle \, ds \, ds'$$

$$= \int_{s_0}^{s_1} \int_{s_0}^{s_1} e^{-j(\psi(s)-\psi'(s))} R(s-s') \, ds \, ds' \tag{3.74}$$

where $R(s-s')$ = autocorrelation function of $e^{-j\epsilon(s)}$.

By assuming that $p(\epsilon)$ is symmetrical, we may compute these expectations for $g(0,0)$ and $I(0,0)$ where $\psi(s) \equiv 0$. For tractability we take $\epsilon(s)$ as being made up of n independent parts. That is, $p(\epsilon,\epsilon')$ is such that $R(s-s') = 0$ if $s-s'$ is sufficiently large. Then we write

$$\rho = \frac{g(0,0)}{\ell\, a/R} = n \sum_{k=1}^{n} e^{j\epsilon_k} = x + jy \tag{3.75}$$

The factor ℓ is taken as the distance required for $R(s-s')$ to go to zero. R is still range and a is the strength of the scatterer. Defining:

$$\alpha = \langle x \rangle$$

$$s_1 = \text{Var}(x) = \langle x^2 \rangle \tag{3.76}$$

$$s_2 = \text{Var}(y) = \langle y^2 \rangle$$

Clearly,

$$\langle \rho^2 \rangle = \langle x^2 \rangle + \langle y^2 \rangle = s_1 + s_2 + \alpha^2 \tag{3.77}$$

53

and

$$\text{Var}(\rho) = \left\langle \rho^2 \right\rangle - \left\langle \rho \right\rangle^2 = s_1 + s_2 \tag{3.78}$$

For large n, we may use the results of Beckman[18] to write the probability density of ρ

$$p(\rho) = \frac{\rho}{(s_1 s_2)^{1/2}} \, e^{-\frac{\alpha^2}{2s_1} - \frac{s_1 + s_2}{4 s_1 s_2} \rho^2}$$

$$\times \sum_{m=0}^{\infty} (-)^m \, \mathcal{E}_m I_m \left(\frac{s_2 - s_0}{4 s_1 s_2} \rho^2 \right) I_{2m} \left(\frac{\alpha \rho}{s_1} \right) \tag{3.79}$$

where I_m is the modified Bessel function of order m and

$$\mathcal{E}_m = \begin{cases} 1 \,, & m = 0 \\ \\ 2 \,, & m \neq 0 \end{cases} \tag{3.80}$$

The distribution of ϵ determines everything. If ϵ is narrowly distributed then $\alpha \simeq 1$ and ϵ has very little effect. If, however, ϵ is distributed over a large part of 2π, then the mean α is small, while the variances become large. In particular, if the distribution of ϵ is uniform over 2π, or any multiple of 2π, then $p(\rho)$ becomes Rayleigh. For a Gaussian distribution, $p(\rho)$ becomes Rayleigh as the standard deviation approaches a full cycle. When this occurs, everything is lost, since the phase information upon which this method depends is completely destroyed.

D. INTRODUCTION OF THE REFERENCE WAVE

If one considers the results of the previous section in practical terms, it immediately becomes clear that the requisite coherence for

avoiding the detrimental effects of random phase errors is not likely to be achieved directly with independent oscillators. Spacecraft velocities for planetary flybys or orbiters are typically on the order of a few kilometers per second, and altitudes of a few hundred kilometers upward can be expected. Thus, an f ratio on the order of one-tenth requires at least seconds, or even tens of seconds at a minimum, to achieve. If we consider a direct scheme such as that given in Chapter II, Fig. 1, for obtaining the complex signal, then the oscillator used to provide the sine and cosine functions and the source oscillator providing the illuminating wave must be extremely stable. Letting τ represent the time over which the scattered signal is observed, we require that the spectral line of an unmodulated signal have a bandwidth of less than $1/\tau$, after passing through the receiving system. For a carrier frequency of Ω this requires circuits with a Q_o so that

$$Q_o \geq \frac{\Omega \tau}{2\pi} \tag{3.81}$$

in both the transmitter and receiver. As a numeric example, consider a frequency of 1 gc and an observation time of 10 sec. The minimum Q_o required would be 10^{10}.

However, there is a simple expedient that removes this difficulty; that is to use the illuminating wave as it is received directly on board the spacecraft as a reference. This is possible because (1) the direct signal is generally a great deal stronger than the reflected signal and (2) as a result of the spacecraft's motion, the direct signal is usually separated in frequency from the reflected signal. After extraction from the composite direct/scattered signal present at the spacecraft, the direct signal is substituted for the carrier $e^{j\Omega t}$, which we used in our description of the analytic signal, and is used to obtain a complex signal. This may be simply shown by writing the direct and reflected signals as separate parts.

$$e = a_o e^{j(\Omega t - \bar{k}_i \cdot \bar{r})} + \tilde{e}_s(t) \tag{3.82}$$

Obviously, $a_o e^{j(\Omega t - \bar{k}_i \cdot \bar{r})}$ is the direct wave. The $\tilde{e}_s(t)$ is the analytic signal representation of the scattered wave. The effect of this operation is to subtract not only the phase term Ωt, normally associated with the complex signal, but an additional $-\bar{k}_i \cdot \bar{r}$ as well. Thus, the signal from the ith target becomes

$$E_i = a_i e^{j(\varphi_i + \bar{k}_i \cdot \bar{r})} \tag{3.83}$$

Since all targets are equally affected, the analysis of the resolution cell is undisturbed. We merely subtract the $-\bar{k}_i \cdot \bar{r}$ from the expanded phase and continue as before. Even the arguments for the effects of errors hold virtually unchanged.

The oscillator stability requirements are relaxed considerably by use of the direct wave. Suppose that the transmitter phase jitter is given by a random term $\phi_\epsilon(t)$ added to its Ωt variation.

$$\varphi = \Omega t - \bar{k}_i \cdot \bar{r} + \phi_\epsilon(t)$$

While the phase of the reflected signal is

$$\varphi = \Omega t - \bar{k}_{\bar{p}_i \bar{r}} \cdot (\bar{r} - \bar{p}_i) + \phi_\epsilon(t - \triangle) \tag{3.84}$$

The term

$$\triangle t = \frac{(\bar{r} - \bar{p}_i) \cdot \bar{u}_{\bar{p}_i \bar{r}} - |\bar{p} - \bar{r}|}{c}$$

gives the total differential time delay along the direct and reflected paths, neglecting second order retardation, as illustrated in Fig. 17.
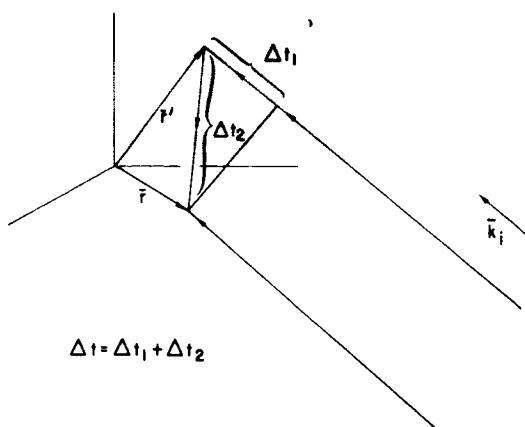
FIG. 17.   TOTAL DELAY PATH.

$\Delta t = \Delta t_1 + \Delta t_2$

After performing the operations of Fig. 10, the analytic signal from a point target becomes

$$E_i = \frac{a_i}{|\bar{r}-\bar{p}_i|} e^{j(\phi_i + \bar{k}_i \cdot \bar{r} + \phi_\epsilon(t) - \phi_\epsilon(t-\Delta t))} \qquad (3.85)$$

To the extent that $\phi_\epsilon(t)$ and $\phi_\epsilon(t-\Delta t)$ are correlated, the variations that they represent cancel out. Furthermore, this is independent of the length of the observation time τ. Again, requiring that Q_o be large enough to guarantee the needed stability,

$$Q_o \geq \frac{\Omega}{2\pi} \frac{\Delta t}{c} = \frac{(\bar{r}-\bar{p}_i) \cdot \bar{u}_{\bar{p}_i \bar{r}} - |\bar{r}-\bar{p}|}{\lambda} \qquad (3.86)$$

Therefore, the oscillator stability now goes directly as the path length difference in wavelengths. The distance associated with this Q_o, $c/\Delta t$ is referred to as the coherence length of the oscillator.

E.   THE OUTPUT SIGNAL-TO-NOISE RATIO

Assuming that our radar is operating within the restrictions for preserving phase coherence, all the errors considered so far have represented imperfections in our knowledge of the experimental parameters

under which our data are taken, with the conclusion that the principal effects can be summed up as a distortion of the coordinate system to which the recovered data are referred. However, the most severe problem to be expected in any form of planetary radar is that of overcoming the receiver noise with signals that have propagated over extreme ranges and are received only after reflection from the surface of a planet. Therefore, the scattered signal exists in the presence of additive thermal noise, and the processor must act on signal and noise simultaneously. This is the situation we shall now consider for the point target. For convenience in describing the noise, the signals will be considered in the time domain.

The method of recovery has been to multiply by the complex conjugate of the expected signal from a given target and to integrate. Thus, if, as before, the composite signal is $E(t)$, then the processor may be written as a convolution with the expected signal from each portion of the surface, sampled at the appropriate time

$$\alpha \int_{t_0}^{t_1} E(t)E_i^*(t)dt = \alpha \left. \int_{t_0}^{t_1} E(\tau)E_i^*(t-\tau)dt \right|_{\tau=0} \tag{3.87}$$

where α is an arbitrary gain factor. This may be modeled as a bank of linear filters with impulse response $E_i^*(-\tau)$, $-t_1 < \tau < -t_0$ sampled at $\tau = 0$.
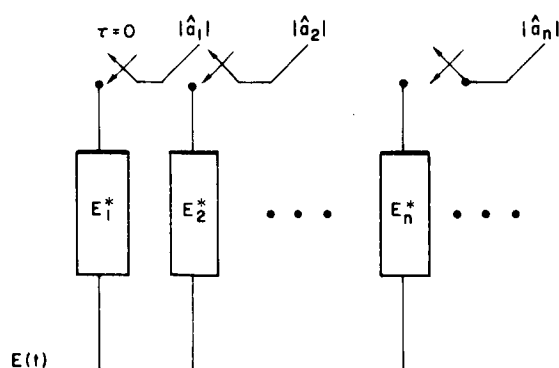

FIG. 18. PARALLEL FILTER MODEL FOR PROCESSOR.

Now, to $E(t)$ we add white noise with complex envelope $N(t)$ so that for a single filter, our model becomes
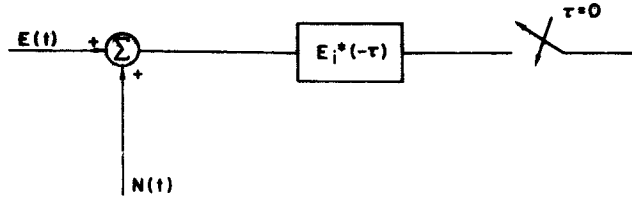
FIG. 19. ADDITION OF NOISE TO PROCESSOR.

If we let $G_i(\omega)$ be the transfer function of the filter with impulse response $E_i(t)$ and assume that the noise is a stationary random process, the output noise power density is $N_o/2 \, |G_i|^2 \, \alpha^2$, and the output noise power is just the density integrated over frequency,

$$\text{Noise Power out} = \alpha^2 \, \frac{N_o}{2} \int_{-\infty}^{+\infty} |G_i(\omega)|^2 \, d\omega \qquad (3.88)$$

By the convolution theorem, the filter response to $E_i(t)$ itself may be expressed as

$$\alpha \int_{-\infty}^{+\infty} G_i(\omega) \, G_i^*(\omega) \, e^{-j\omega\tau} \, d\omega \qquad (3.89)$$

when $\tau = 0$, the ratio of the output powers is

$$\frac{S}{N} = \frac{\left[\alpha \int_{-\infty}^{+\infty} |G_i|^2 \, d\omega \right]^2}{\frac{N_o}{2} \alpha^2 \int_{-\infty}^{+\infty} |G_i(\omega)|^2 \, d\omega} = \frac{\int_{-\infty}^{+\infty} |G_i(\omega)|^2 \, d\omega}{N_o/2} \qquad (3.90)$$

Recognizing that the integral in the numerator of the right-hand side is just the energy contained in the signal,

SEL-67-042

$$E = \int_{-\infty}^{+\infty} |G_i(\omega)|^2 \, d\omega \qquad (3.91)$$

gives

$$\frac{S}{N} = \frac{2E}{N_o} \qquad (3.92)$$

Filters with an impulse response which is proportional to a reversed version of the complex conjugate function of a given signal (or equivalently, have a transfer function which is the complex conjugate), are said to be matched to that signal.[19] This definition certainly applies to what has been done here. A well-known property of such filters is that they maximize the output signal-to-noise in a mean square sense, and that the signal-to-noise ratio depends only on the energy in the signal and the spectral density of the noise as given by Eq. 3.92.

IV. THREE PHYSICAL INTERPRETATIONS

A. SYNTHETIC ARRAY

Suppose that instead of a spacecraft recording signals along its trajectory, we consider the construction of an array of infinitesimal antennas, co-linear with the trajectory, as in Fig. 20.
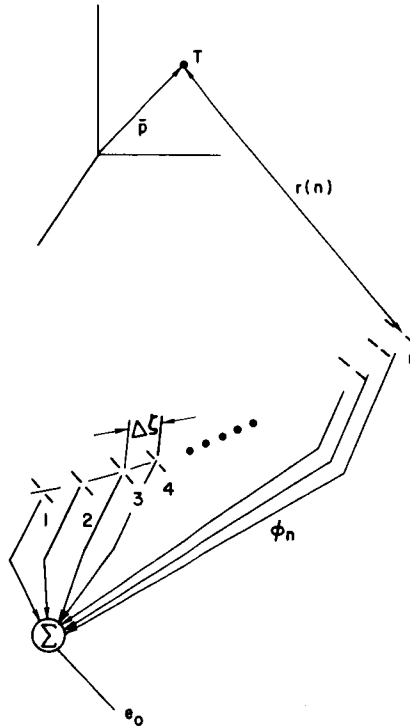

FIG. 20. THE ARRAY ANALOGY.

The scattered fields arriving at each element of our array would be the same as before and given by:

$$e(t,n) = \frac{a\, e^{-j[\Omega t - kr(n)]}}{r(n)} \tag{4.1}$$

In Eq. 4.1, we suppose that all the elements are equally spaced with distance $\Delta\zeta$, and $r(n)$ is the distance from the target to the nth element. If ϕ_n is the phase shift associated with the transmission line running from the nth element to the summing point and the elements

SEL-67-042

have equal gain, then the output of the array is

$$e_o = e^{j \Omega t} \, a \sum_1^N \frac{e^{-j[k \, r(n) + \phi_n]}}{r(n)} \qquad (4.2)$$

The magnitude of e_o has a maximum if the ϕ_n are chosen so that

$$kr(n) + \phi_n = \text{constant for all} \quad n$$

or

$$\phi_n = -k \, r(n) + c \qquad (4.3)$$

Substituting this result in Eq. 4.2 we obtain

$$|e_o| = |a| \left| \sum_1^N \frac{e^{-j[kr(n)] - kr(n)]}}{r(n)} \right|$$

$$= a \sum \frac{1}{r(n)} \simeq \left| \frac{a}{R} \right| N \quad \text{if} \quad R \simeq r(n) \qquad (4.4)$$

However, the multiplication by $e^{+jkr(n)}$ and the summation of the contributions along the path are precisely the operations we introduced in Chapter III for the recovery of the $|a|$. The phase delay introduced by the connecting transmission lines corresponds to the multiplication by $e^{jkr(n)}$, while the connection at the summing point performs the integration. The difference is that whereas an array simultaneously samples and sums the incoming fields along the entire path, the spacecraft can only sequentially determine the amplitude and phase field at each point and in some way record the result so that the weighting by the proper phase factor and integration may be done later. In terms of this analogy, the use of the reference wave in Chapter II is just a device for calibrating the phase measurement.

The usefulness of this interpretation is limited by the parameters of our analysis. Since we are always interested in path lengths that are a significant fraction of the range at the point of closest approach, we must always deal with spherical wavefronts from our targets. In fact, it is the different curvature of the wavefronts from various ranges that gives us resolution in depth. Thus, our targets always lie in the near field of the array. Consequently, one of the more powerful tools of antenna theory, the Fourier transform relations between the fields in the aperture of an antenna and its radiation pattern, cannot be applied directly to our problem. Still, the idea that the processing represents an array focused at close range is a useful concept.[20,21,22,23]

B. THE TRACKING FILTER

We have previously considered the inversion as being made up of two distinct operations, one where the data are collected by heterodyning the scattered signals with the incident wave, and a second operation where we correct the data for the phase changes from a given target as a function of position and integrate the result. For purposes of calculation and data interpretation, the geometrical approach adopted in Chapter III proves itself most powerful.

However, perhaps the simplest approach to understanding the processing for a point target in familiar terms is derived from a consideration of the time-frequency characteristics of the signal scattered from a point as the spacecraft goes by, and the changes in the processor for the same time period. This is the interpretation we shall now explore.

Re-drawing a simplified block diagram for processing the data from a single point with the signals as explicit functions of time, we have
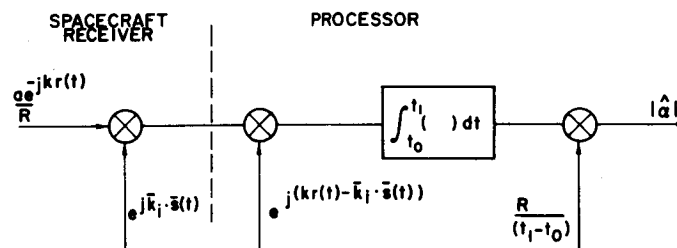
FIG. 21. SIMPLIFIED PROCESSOR.

The function $e^{jkr(t)}$ is again the distance from a target to the spacecraft at t and $\bar{s}(t)$ is the change in spacecraft position we introduced in Eq. 2.61. Fig. 22 gives the geometry.
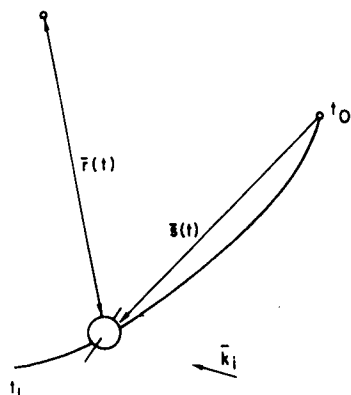

FIG. 22. THE SIMPLIFIED GEOMETRY.

Recognizing that the reference signal $e^{j\bar{k}_i \cdot \bar{s}(t)}$ functions only as a means of providing a coherent reference signal necessary for practical reasons, we may give a mathematically equivalent diagram with only one frequency multiplication.
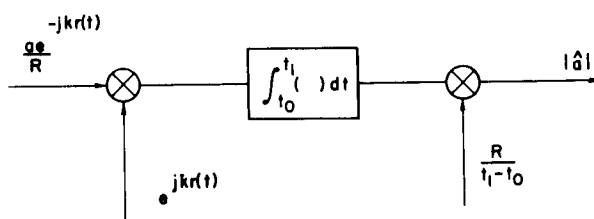
FIG. 23. TRACKING FILTER FORMULATION.

The overall effect is to extract continuously the Doppler shift associated with a particular target and to integrate the result for a time $t_1 - t_0$. In the frequency domain, this corresponds to tracking continuously the target signal with a narrow-band filter whose passband is on the order of $1/(t_1 - t_0)$ Hz.

It is a simple matter to verify our signal-to-noise ratio calculations. The signal power out is $|a|^2$ while the noise power is $kTB/2$, where $B = 1/t_1 - t_0$. Therefore

$$\frac{S}{N} = \frac{|a|^2}{\frac{kT}{2}\frac{1}{\tau}} = \frac{2E}{N_o} \qquad (4.5)$$

as before.

This approach also provides some additional insight into the resolution mechanism, particularly resolution in range. Using our straight line approximation to the flyby:

$$r = \{R^2 + x^2(t)\}^{\frac{1}{2}}$$

$$\dot{r} = \frac{xv(t)}{r} \qquad (4.6)$$

Multiplying by $2\pi/\lambda$, we have the instantaneous frequency shift of

$$\omega = -2\pi \frac{v}{\lambda} \cdot \frac{x/R}{\left(1 + (x/R)^2\right)^{\frac{1}{2}}} \qquad (4.7)$$

For a single target this gives the S-shaped curve plotted in Fig. 24.
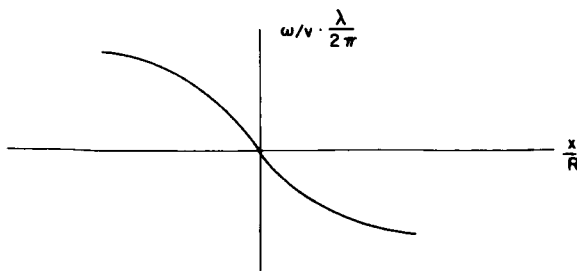

FIG. 24. TIME-FREQUENCY SIGNAL TRACKS.

As we have already seen, the recovery of the signal that follows this curve is accomplished by continuously tracking this signal with a narrow-band filter over some fraction of the trajectory. Signals from other targets are rejected by this mechanism. Suppose that there are just two targets present, neither of which is at the origin of our coordinate system. For convenience, take one as displaced parallel to our trajectory and the other as displaced in a direction normal to the trajectory. The trajectories of these two points and filter tracking the origin are all given in Fig. 25. Clearly the resolution parallel to the path can be
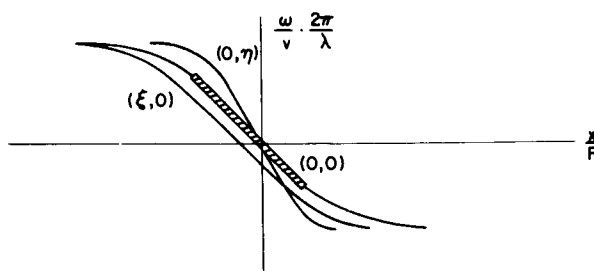

FIG. 25. TIME-FREQUENCY TRACKS AND THE TRACKING FILTER.

quite good, since only a slight displacement in the ξ direction is required in order that the signal avoid the filter passband altogether. In the η-direction, however, the signal always passes through the filter, so there will always be some contribution to the output from this target, although its relative strength may become quite small when the filter tracks the desired signal for a longer and longer time.

One other important property of the method is revealed by this formulation. As x/R becomes larger,

$$\omega \rightarrow 2\pi \frac{v}{\lambda} \tag{4.8}$$

for all targets near the origin. Thus, if the filter is made to track a given signal too close to its asymptotic values, then resolution is lost as the signals from other targets approach the same asymptote.

C. THE HOLOGRAM ANALOGY AND OPTICAL RECONSTRUCTION

The analogs of the antenna array and of the tracking filter demon-
strate a striking connection between spatial and temporal signals, i.e.,
an array integrates in space in a manner that is completely equivalent
to a tracking filter in the time domain. The third analogy is even more
remarkable, in that it provides an automatic method for performing all
the operations implied by the first two for all targets simultaneously.
Furthermore, it is easily explained in terms of the expression with which
this work really began, Eq. 2.38 of Chapter II:

$$E_s(\bar{r}) = \frac{\mu}{4\pi} \int_s \frac{K(r') \, e^{-jk|\bar{r}-\bar{r}'|}}{|\bar{r}-\bar{r}'|} \, ds \qquad (4.9)$$

We wish to apply this expression to diffraction phenomena that occur
as the result of a plane wave propagating through a two-dimensional medium
of varying transmission. We assume that there are no spatial variations
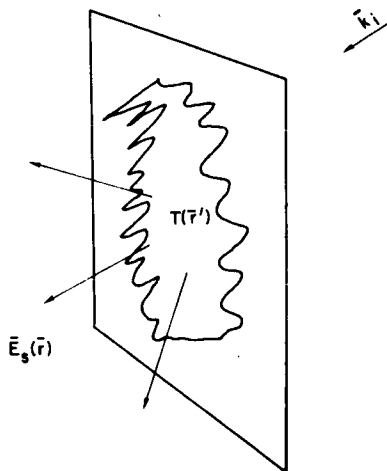in phase associated with the medium. That is, in Fig. 26,,if $e^{-j\bar{k}_i \cdot \bar{r}}$

FIG. 26. SCATTERING BY A
TRANSMITTING SCREEN.

is the incoming plane wave, and $T(\bar{r})$ is the transmission coefficient
of the screen and is real, then immediately after passing through the
screen, the outgoing wave is

$$E_i(\bar{r}') = T(\bar{r}') \, e^{-j\bar{k}_i \cdot \bar{r}'} \tag{4.10}$$

The integral formulation of the scattered wave may be applied by substituting the displacement current associated with $E_i(\bar{r}')$

$$K(\bar{r}') = j\omega\epsilon \, E_i(\bar{r}') \tag{4.11}$$

for current density. The integral must be evaluated on a surface when the currents are known, so we take, as the surface of integration, a plane lying just above the diffracting screen. Except for an unimportant constant, the field at any point beyond the screen is then given by Eq. 4.12

$$E_s(\bar{r}) = \int_s \frac{\bar{E}_i(\bar{r}') \, e^{-jk|\bar{r}-\bar{r}'| - j\bar{k}_i \cdot \bar{r}'}}{|\bar{r}-\bar{r}'|} \, ds \tag{4.12}$$

For the proper choice of $\bar{r}$, the integral is identical to the Eq. 3.20 we developed for recovery of the amplitude from a point source.

Suppose that $T(\bar{r}')$ is made to correspond to the data taken by our spacecraft. Since any orbit is always a plane curve, this can always be accomplished by scaling the orbit onto the diffracting screen, and causing the transmission along the scaled orbit to vary with the data.

Elsewhere, the screen must be opaque. The data must be in a real form, such as that given by Eq. 4.13, for a point source originally at $\bar{p}$.

$$\overline{T}(\bar{r}') = \left\{ \frac{e^{+j(k|\bar{r}'-\bar{p}|+\bar{k}_i \cdot \bar{r}')}}{|\bar{r}'-\bar{p}|} + \frac{e^{-j(k|\bar{r}-\bar{p}|-\bar{k}_i \cdot \bar{r}')}}{|\bar{r}'-\bar{p}|} \right\}^{1/2} \tag{4.13}$$

If the wave number of the illuminating wave is now scaled by the same factor and given a direction that corresponds to the negative of
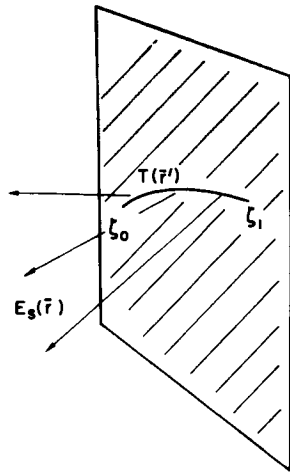
FIG. 27. TRANSMITTING SCREEN
WITH SPACECRAFT DATA.

the original reference wave, Eq. 4.12 with $T(\bar{r}')$ given by Eq. 4.13 becomes

$$
E_s(\bar{r}) = \frac{1}{2} \int_{\substack{\text{scaled} \\ \text{trajectory}}} \frac{e^{+j(k|\bar{r}'-\bar{p}|-k_i \cdot r')}}{|\bar{r}'-\bar{p}|} \cdot \frac{e^{-j(k|\bar{r}-\bar{r}'|+k_i \cdot \bar{r}')}}{|\bar{r}-\bar{r}'|} \, ds \qquad \text{I}
$$

$$
+ \frac{1}{2} \int_{\substack{\text{scaled} \\ \text{trajectory}}} \frac{e^{-j(k|\bar{r}'-\bar{p}|-\bar{k}_i \cdot \bar{r}')}}{|\bar{r}'-\bar{p}|} \cdot \frac{e^{-j(k|\bar{r}-\bar{r}'|+\bar{k}_i \cdot \bar{r}')}}{|\bar{r}-\bar{r}'|} \, ds \qquad \text{II}
$$

$$(4.14)$$

If $\bar{r} = \bar{p}$, part I of this expression is identical to the starting integral for the calculation of the image point response. Part II represents a spurious response. The intensity of the diffracted electric field due to I exactly recreates $\bar{r}$, the image point response we calculated in Chapter II.

Furthermore, the response occurs at the point in space that corresponds to the original target position. We must be a little careful. The important portion of the integral is the function $\bar{r} - \bar{r}'$ in the exponent of the kernel. As was pointed out in the original discussion of the image point response, all targets lying on the same circle about

69

the original trajectory produce a response at the same position, since they are all related to the trajectory through the same phase function. It is only by knowing the location of the target surface that we are able to map the surface brightness distribution.

Now we have the opposite situation. For a straight line trajectory, the diffraction screen reproduces a bright spot not only at the original point, but at every point on a circle centered on $T(\bar{r})$ that contains that point. However, if we sample the field intensity on a surface that has the same geometrical relationship to the $T(\bar{r})$ as our planetary surface had to the original spacecraft trajectory, we will recover the surface brightness distribution spatially undistorted, albeit, it is convolved with our point response function. It is a simple matter to show that for a collection of point scatters, the surface brightness distribution is convolved with the point response in the reconstruction. Because our functional relationship has remained unchanged, the noise behaves in exactly the same manner as before and processing gain is retained.

An interesting point is that when $\bar{r}$ is far removed from $\bar{r}'$, so that the vector directions $(\bar{r}-\bar{r}')$ and $(\bar{p}-\bar{r}')$ are approximately the same, the integral becomes

$$I \rightarrow \frac{e^{-jk|\bar{r}-\bar{p}|}}{|\bar{r}|-|\bar{p}|} \int_{\substack{\text{scaled} \\ \text{trajectory}}} (1)\ ds \qquad (4.15)$$

which looks like a plane wave originating at $\bar{p}$. This approximation always applies to II, since $-\bar{p}$ represents a point behind, i.e., on the side of the illuminating wave, the diffracting screen. Therefore, II represents a uniform background intensity that apparently comes from a point source behind the slit. An obvious method for avoiding this background contribution is to choose the geometry so that the real response, due to I, falls outside the wave due to II.

There is nothing in our derivation thus far that is critical in terms of frequency. Herein lies a possibility for analog reconstruction of the surface brightness. By scaling the data from radio to optical

frequencies, it becomes possible to create a diffracting slit, such as we have described, by scanning photograph plates with a beam of light, intensity-modulated in this manner automatically generates the diffraction pattern we have been discussing. A second photographic plate, placed in the original target plane, as in Fig. 28, scaled by the same factor, will then automatically record the reconstructed brightness distribution.
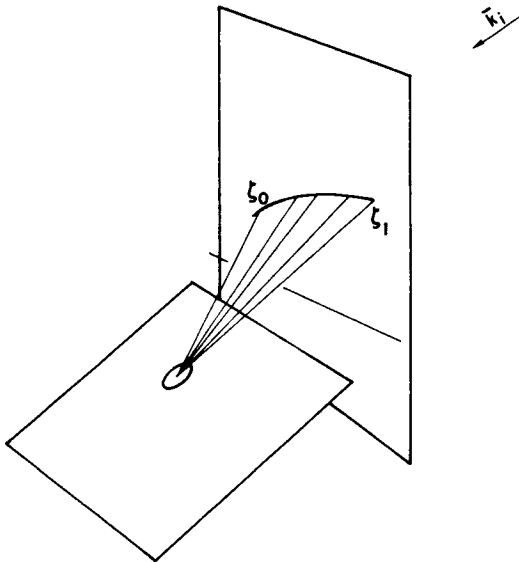
FIG. 28. RECONSTRUCTION VIA TRANSMITTING SCREEN.

A two-dimensional diffracting screen with $T(r)$ corresponding to the intensity of the interference pattern generated by a coherent source of illumination and a scattered wave is called a hologram. It is easy to show that the interference pattern contains, in addition to several spurious products, the same data that our spacecraft collects in one dimension by product detection.[24] Much of the theory of holograms is germane to the reconstruction of the surface brightness distribution and has been discussed elsewhere.[24,25,26]

V. RELATIONSHIP BETWEEN THE RESOLUTION CELL AND SIGNAL-TO-NOISE RATIO

A. PROCESSOR FOR MAXIMUM-LIKELIHOOD ESTIMATE

The conventional radar problem rather naturally divides itself into two parts: (1) the detection problem, where one is concerned with deciding when a target signal is present in a background of noise, and (2) the resolution problem, where, usually with the assumed absence of noise, one is concerned with fundamental limits on the radar's ability to discriminate between closely spaced targets. When stated in this way, the radar problem is extremely well understood and we have drawn upon ideas of detection and resolution in calculating the signal-to-noise ratio and image point response.

A little reflection will show, however, that the ordinary development of the detection and resolution problem cannot be carried much further here. Detection, in the sense of determining the presence or absence of a target is completely out of place, because one of the major assumptions of this report is that the target is known to exist and moreover that our knowledge of its position involves only a small uncertainty. A straightforward application of the resolution cell results is inappropriate because the assumptions of high signal-to-noise ratios made in most developments and of a knowledge of the target environment are generally never true for the applications envisioned. Nevertheless, we shall still find the developments of Chapter III extremely valuable later on.

And so, we take a more abstract approach. This time, we assume that the brightness distribution over the surface is a random process generated in some unknown manner by the interaction of the incident wave and the surface itself. Further, assume that we measure the scattered fields at our spacecraft as before, and that the relationship between the scattered fields and the current distribution is known and is given by our integral expression Eq. 2.38. What, then, is the best estimate of the surface brightness distribution averaged over some area, and how does the quality and form of the estimate vary with the size of the area itself, the statistical parameters of the brightness distribution and the noise? In other words, how does one trade resolution for signal-to-noise ratio?

Probably the most difficult portion of this problem is the selection of a stochastic model for the surface with some basis in reality, but which is tractable at the same time. Almost any presumption about the surface is likely to be wrong. Therefore, one is led to select some model for the surface, derive the expression for an estimate on the basis of the model, and then examine the sensitivity of the formulation to the original assumptions. This is the goal of this chapter.

We begin by assuming that the current distribution has the same basic character everywhere, but that for one reason or another, varies in amplitude from place to place. Such an assumption might be based on the belief that the same sorts of material stresses and strains act to roughen the entire surface but that the brightness varies from place to place because of shadowing or variations in the electromagnetic properties of the material.

Designating the complex surface current distribution as $a(\xi,\eta)$, we define the average brightness over the area $\mathcal{S}$ by

$$A^2 = \frac{1}{\mathcal{S}} \int_{\mathcal{S}} (a)^2 \, d\xi \, d\eta \qquad (5.1)$$

and then take

$$\gamma(\xi,\eta) = a(\xi,\eta)/A \qquad (5.2)$$

so that

$$\frac{1}{\mathcal{S}} \int_{\mathcal{S}} |\gamma|^2 \, d\xi \, d\eta = \frac{1}{\mathcal{S}} \int_{\mathcal{S}} \frac{|a(\xi,\eta)|^2}{A^2} = 1 \qquad (5.3)$$

The quantity A then is fixed for any given $\mathcal{S}$. Introducing the geometry given in Fig. 29, the signal received along the trajectory ζ may be obtained from Eq. 2.38. Designating the kernel by $f(\zeta;\xi,\eta)$ and
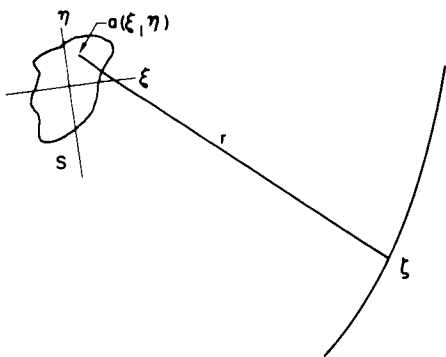
73

FIG. 29. GENERAL GEOMETRY FOR
EXPANDED RESOLUTION CELL.

neglecting the constants $f(\zeta;\xi,\eta) = \dfrac{e^{-jkr}}{r}$, and

$$v(\zeta) = \int_{\mathcal{A}} a(\xi,\eta)\, f(\zeta;\xi,\eta)\, d\xi\, d\eta = A \int_{\mathcal{A}} \gamma(\xi,\eta)\, f(\zeta;\xi,\eta)\, d\xi\, d\eta \quad (5.4)$$

so that the received signal is

$$s(\zeta) = v(\zeta) + N(\zeta) \tag{5.5}$$

where $N(\zeta)$ is the complex envelope of the receiver noise when the space-craft is at position ζ. The quantity $N(\zeta)$ is taken as stationary, white, and Gaussian.

Autocorrelation will be designated by ϕ with a prefix to indicate the corresponding variable. Thus

$$_\gamma\phi(\xi,\xi',\eta,\eta') = \left\langle \gamma(\xi,\eta)\, \gamma^*(\xi;\eta') \right\rangle = {_\gamma}\varphi(\rho)$$

so that

$$_a\varphi = A^2 \, {_\gamma}\varphi \quad \text{where} \quad \rho^2 = (\xi-\xi')^2 + (\eta-\eta')^2 \tag{5.6}$$

and

$$_n\varphi(\xi,\zeta') = N_o\delta(\zeta-\zeta')$$

$$_v\varphi(\xi,\zeta') = \langle v(\zeta)\, v^*(\zeta')\rangle$$

$$_s\varphi(\zeta,\zeta') = \langle s(\zeta)\, s^*(\zeta')\rangle = {}_n\varphi + {}_v\varphi$$

The autocorrelation function of $v(\zeta)$ is calculated from

$$_v\varphi = \langle v(\zeta)v(\zeta')\rangle = A^2\int_{\mathcal{S}}\int_{\mathcal{S}'}\gamma(\xi,\eta)\gamma^*(\xi,\eta)f(\zeta;\xi,\eta)\,f^*(\zeta;\xi,\eta')\,d\xi d\eta d\xi'd\eta'$$

$$= A^2\int_{\mathcal{S}}\int_{\mathcal{S}}{}_\gamma\varphi\; ff^*d\xi d\eta d\xi'd\eta' \qquad (5.7)$$

The term $_\gamma\varphi$ is clearly Hermitian and it is a simple matter to show that $_v\varphi$ is also. Let g_μ be an eigenfunction of $_v\varphi$ so that

$$\int g_\mu\, g_\nu^* = \delta_{\mu\nu} \qquad (5.8)$$

and

$$\lambda_\mu\, g_\nu = \int {}_v\varphi g_\nu^*\, d\xi \qquad (5.9)$$

The function $_v\varphi$ is also positive-definite since

$$\left\langle\left|\int h(t)\, v(t)\, dt\right|^2\right\rangle = \iint h(t)\, h^*(t')\langle v(t)\, v^*(t')\rangle dt\, dt'$$

$$= \iint h(t)\, h(t')\, {}_v\varphi(t,t')\, dt\, dt' > 0 \qquad (5.10)$$

for all $h(t)$.

Therefore, by positive definiteness and Hermitian properties of $_v\varphi$, the λ_μ are positive and real. It follows from Mercer's[27,28] theorem that the autocorrelation function may be expanded in terms of its own eigenfunction as

$$_v\varphi = \sum_1^\infty \lambda_\mu \, g_\mu \, g_v^* \tag{5.11}$$

For

$$S_\mu = \int g_\mu^* S = (g_\mu^*, S) = X_\mu + Y_\mu \tag{5.12}$$

we have

$$\langle S_\mu S_v^* \rangle = \iint g_\mu^* g_v \langle SS^* \rangle dt \, dt' = 2(A^2 \lambda_\mu + N_o)\delta_{\mu v} \tag{5.13}$$

thus

$$\langle S_\mu S_v^* \rangle \equiv 0 \tag{5.14}$$

A linear operation on a Gaussian variable produces another Gaussian variable. Thus the S_μ are independent, Gaussian random variables of zero mean and

$$\langle |S_\mu|^2 \rangle = \langle X_\mu^2 \rangle + \langle Y_\mu^2 \rangle = 2(A^2 \lambda_\mu + N_o) \tag{5.15}$$

which implies

$$p(\overline{S}/A^2) = \prod^\infty \frac{1}{2\pi(A^2 \lambda_\mu + N_o)} e^{-\sum_1^\infty \frac{|S_\mu|^2}{2(A^2 \lambda_\mu + N_o)}} \tag{5.16}$$

To obtain a maximum likelihood estimate, we require

$$\frac{\partial}{\partial A^2} \, p(\overline{S}|A^2) = 0 \tag{5.17}$$

In turn,

$$\sum_1^\infty \frac{\lambda \, [\,|S_\mu|^2/2 - (A^2\lambda_\mu + N_o)\,]}{(A^2\lambda_\mu + N_o)^2} = 0 \tag{5.18}$$

This relation has also been given by Hofstetter[29] for a similar estimation problem, starting from our Eq. 5.5.

In general, Eq. 5.18 cannot be solved for A^2. However, we make some progress by expressing our estimate of A^2, $\hat{A}^2$ in terms of A^2 itself

$$\hat{A}^2 = \frac{\displaystyle\sum_1^\infty (|S_\mu|^2/2 - N_o) \frac{\lambda_\mu}{(N_o + A^2\lambda_\mu)}}{\displaystyle\sum_1^\infty \frac{\lambda_\mu^2}{(A^2\lambda_\mu + N_o)^2}} \tag{5.19}$$

or

$$\hat{A}^2 = \frac{\displaystyle\sum_1^\infty (|S_\mu|^2/2 - N_o) \frac{\lambda_\mu}{(N_o/A^2 + \lambda_\mu)^2}}{\displaystyle\sum_1^\infty \frac{\lambda_\mu^2}{(N_o/A^2 + \lambda_\mu)^2}}$$

where

$$\frac{N_o}{A^2} \quad \text{is} \quad \frac{(\text{noise power per unit bandwidth})}{(\text{signal power per unit surface area})}$$

This will become a critical parameter.

Substituting for $|S_\mu|^2$ from Eq. 5.13

$$\hat{A}^2 = \frac{\displaystyle\sum_1^\infty (A^2\lambda_\mu + N_o - N_o)^2 \frac{\lambda_\mu}{(A^2\lambda_\mu + N_o)^2}}{\displaystyle\sum_1^\infty \frac{\lambda_\mu^2}{(A^2\lambda_\mu + N_o)^2}} = A^2 \qquad (5.20)$$

so the estimate is unbiased, at least as long as our choice of A^2 in the processing is correct.

While the general variability of the processor form with changing values of A^2 is of great interest, the case of special interest to us is

$$\frac{N_o}{A^2} \gg 1 \qquad (5.21)$$

so that the estimator becomes

$$\hat{A}^2 = \frac{\displaystyle\sum_1^\infty (|S_\mu|^2/2 - N_o)\,\lambda_\mu}{\displaystyle\sum_1^\infty \lambda_\mu^2} \qquad (5.22)$$

For this case, the variance of the estimate is easily shown to be

$$
\mathrm{Var}(\hat{A}^2) = \frac{\sum_1^\infty (N_o + A^2\lambda_\mu)^2 \lambda_\mu^2}{\left[\sum_1^\infty \lambda_\mu^2\right]^2} = \hat{A}^2 \frac{\sum_1^\infty (N_o/A^2 + \lambda_\mu)^2 \lambda_\mu^2}{\left[\sum_1^\infty \lambda_\mu^2\right]^2} \qquad (5.23)
$$

Hofstetter has computed the efficiency for this case with the result that

$$
\mathrm{eff} = \frac{\left[\sum \lambda_\mu^2\right]^2}{\sum_1^\infty \left(1 + \frac{A^2\lambda_\mu}{N_o}\right)^2 \lambda_\mu^2 \sum_1^\infty \frac{\lambda_\mu^2}{\left(1 + \frac{A^2}{N_o}\lambda_\mu\right)^2}} \to 1, \quad \frac{N_o}{A^2} \to \infty \qquad (5.24)
$$

so that for N_o/A^2 large, this estimate approaches the Cramer-Rao lower bound for the variance of the estimate.

The estimator is basically

$$
\hat{A}^2 = k \sum_1^\infty |S_\mu|^2 \lambda_\mu \qquad (5.25)
$$

Again, for the case of interest, the variance is

$$
\mathrm{Var}\ \hat{A}^2 \to \frac{N_o \sum_1^\infty \lambda_\mu^2}{\left[\sum \lambda_\mu^2\right]^2} \qquad (5.26)
$$

79

The estimator will be recognized as the Hilbert quadratic form

$$\hat{A}^2 = k \int_{t_0}^{t_1} \int_{t_0}^{t_1} s(t)\, \varphi^*(t,t')\, s^*(t')\, dt\, dt' \qquad (5.27)$$

Now by Eq. 5.11

$$\sum_{1}^{\infty} \lambda_\mu^2 = \iint \left(\sum_{1}^{\infty} \lambda_\mu g_\mu g_\mu^* \quad \sum_{1}^{\infty} \lambda_\nu g_\nu^* g_\nu \right) dt\, dt'$$

$$= \iint {}_\nu\varphi\, {}_\nu\varphi^*\, dt\, dt' = \iint \left| {}_\nu\varphi \right|^2 dt\, dt' \qquad (5.28)$$

so that

$$\text{Var } \hat{A}^2 = \frac{N_o^2}{\iint |\varphi|^2\, dt\, dt'} \qquad (5.29)$$

and

$$\frac{\text{Var } \hat{A}^2}{(\hat{A}^2)^2} = \left(\frac{N_o}{A^2} \right)^2 \frac{1}{\iint |\varphi|^2\, dt\, dt} \qquad (5.30)$$

The autocorrelation function is the important ingredient. Maximum-likelihood processing consists, at low signal-to-noise ratio, of matching the processing filter not to the expected signal, but to the expected autocorrelation function.

B. CALCULATION OF SOME SIGNAL AUTOCORRELATION FUNCTIONS

Having determined the general form of the estimator in a fairly unrestricted manner, we are now obliged to make some assumptions about the surface in order to proceed further. Since, as has already been pointed out, the usefulness of any of the results depends on the sensitivity (or rather insensitivity) of the estimator to our surface model, several different cases will be considered.

The estimator is a time-varying filter whose impulse response is equal to the expected autocorrelation function of the scattered signal As before

$$_v\varphi(\zeta,\zeta') = \int_\mathcal{S}\int_\mathcal{S} \,_\gamma\varphi(\xi'-\xi',\eta,-\eta') \, f(\zeta;\eta,\eta) \, f^*(\xi';\xi;\eta') \, d\xi \, d\eta \, d\xi' \, d\eta'$$

$$(5.31)$$

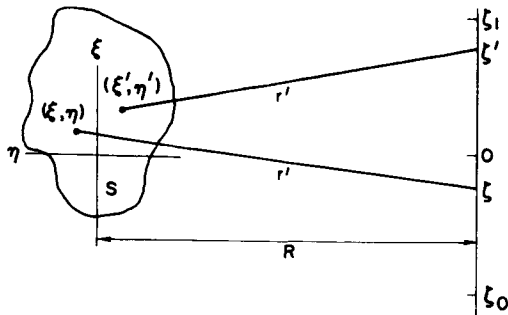where the various terms are defined by Fig. 30 below, and we have assumed a linear trajectory once more.

FIG. 30.   LINEAR GEOMETRY FOR EXPANDED RESOLUTION CELL.

The quantities f are given by

$$f(\zeta;\xi,\eta) = \frac{e^{-jkr}}{r}$$

and

$$(5.32)$$

$$f^*(\zeta';\xi',\eta') = \frac{e^{jkr'}}{r'}$$

Considering the most extreme case first, we take

$$\gamma^\varphi = \delta(\rho) \ , \quad \rho^2 = (\Delta\zeta^2 + \Delta\eta^2)$$

and (5.33)

$$\Delta\zeta = \xi - \xi'$$

$$\Delta\eta = \eta - \eta'$$

This would correspond to a "white" surface.   We have

$$_v\varphi(\zeta,\zeta') = \int_{\mathcal{A}} \int_{\mathcal{A}} \delta(\rho) \ \frac{e^{-jk(r-r')}}{rr'} \ d\xi \ d\eta \ d\xi' \ d\eta'$$

$$= \int_{\mathcal{A}} \frac{e^{-jk(r(\zeta;\xi,\eta) \ - \ r'(\zeta';\xi,\eta))}}{rr'} \ d\xi, \ d\eta$$

$$_v\varphi(\zeta,\zeta') \rightarrow \frac{e^{-jk(r(\zeta;\xi,\eta) \ - \ r'(\zeta';\xi,\eta))}}{rr'} \ \Delta s$$

as

$$\mathcal{A} \rightarrow \Delta s \qquad (5.34)$$

Thus, as the area goes to zero, we obtain the matched filter used in the image point response. To see this

$$\hat{A}^2 = \int_{\mathcal{A}} ss^*\varphi = \int \frac{s(\zeta) \ s^*(\zeta') \ e^{+j(kr(\zeta) \ - \ r(\zeta'))}}{r,r'} \ d\zeta \ d\zeta'$$

(5.35)

$$= \left| \int \frac{s(\zeta) \ e^{+jkr(\zeta)}}{r} \ d\zeta \right|^2$$

as before.

For this case, the variance is trivial

$$\left|_v\varphi(\zeta,\zeta')\right|^2 = \frac{1}{(rr')^2} \tag{5.36}$$

so that

$$\frac{\text{Var A}}{(A^2)^2} = \left(\frac{N_o}{A^2}\right)^2 \frac{r^2 r'^2}{\displaystyle\iint (1)\ d\zeta\ d\zeta'} = \left(\frac{N_o}{A^2}\right)^2 \frac{1}{(\zeta_1-\zeta_0)^2} = \left(\frac{N_o}{2E}\right)^2 \tag{5.37}$$

Changing δ changes the estimator. Consider δ as a linear region of width $\triangle\eta$ between $\xi = a$, $\xi = b$, $\eta = 0$.

$$_v\varphi(\zeta,\zeta') = \frac{\triangle\eta}{R} \int_{\xi=a}^{\xi=b} e^{-jk(r(\zeta)\ -\ r'(\zeta'))}\, d\xi \tag{5.38}$$

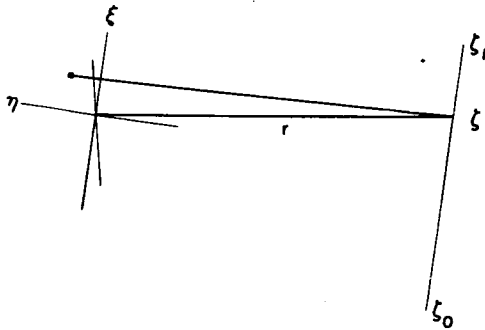Over a short path, the approximations indicated in Fig. 31 are suitable,

FIG. 31. APPROXIMATION FOR EVALUATING CORRELATION FUNCTIONS.

with the result that the path difference is given by

$$\xi\left(\frac{\zeta}{R} - \frac{\zeta'}{R}\right) = (\zeta - \zeta')\,\frac{\xi}{R} \tag{5.39}$$

Therefore,

$$_v\varphi(\zeta,\zeta') = \Delta\eta \int_{\xi_0}^{\xi_1} \frac{e^{ijk((\zeta-\zeta')\xi/R + r(\zeta)-r'(\zeta'))}}{rr'} \, d\xi$$

$$= \Delta\eta \, e^{-jk(r(\zeta)-r'(\zeta'))} \int_{\xi_0}^{\xi_1} e^{+jk(\zeta-\zeta')\xi/R} \, d\xi$$

$$= \Delta\eta \, \frac{e^{-jk(r(\zeta)-r'(\zeta'))}}{rr'} \, \text{sinc}\left\{\frac{\Xi}{R}(\zeta-\zeta')\right\} \Xi \qquad (5.40)$$

where

$$\Xi = \xi_1 - \xi_0$$

A similar extension applies in the η direction. Having integrated over one strip, we need only add up the strips. Again obtaining the approximations from Fig. 31.

$$_v\varphi(\zeta,\zeta') = \frac{e^{-jk(r-r')}}{rr'} \iint e^{jk(\zeta-\zeta;)\xi/R} \, e^{jk\left(\sqrt{\zeta^2+R^2} - \sqrt{\zeta'+R^3}\right)\eta/R} \, d\xi \, d\eta$$

$$= e^{-jk(r-r')} \, \text{sinc}\left[\left(\frac{k\Xi}{R}(\zeta-'\zeta)\right)\right] \text{sinc}\left[\frac{kH}{R}\left(\sqrt{\zeta^2+R^2} - \sqrt{\zeta^2+R^\xi}\right)\right]\Xi$$

where (5.41)

$$= \eta_1 - \eta_0$$

The appearance of the sinc function as a weight on the point processor is interpreted as accounting for beats between different portions of the resolution cell when it is expanded.

But how does the processor change with the autocorrelation function?

$$_\gamma\varphi = e^{-a|\xi-\xi'| - a|\eta-\eta'|} \qquad (5.42)$$

Then

$$_\gamma\varphi = e^{-jk(r-r')} \iint_{\delta}\int_{\delta} e^{-a|\Delta\eta| - a|\Delta\eta|} e^{jk\epsilon} \, d\xi \, d\eta \, d\Delta\xi \, d\Delta\eta \qquad (5.43)$$

as before

$$\epsilon = \sqrt{\frac{\zeta^2+R^2}{R}}\, \eta + \zeta\, \frac{\xi}{R} - \sqrt{\frac{\zeta'^2+R^2}{R}}\, \eta - \zeta'\, \frac{\xi}{R} \qquad (5.44)$$

giving

$$\varphi = \Xi\, H \; \frac{e^{-jk(r-r')} \dfrac{4}{a^2}\, \mathrm{sinc}\left[\dfrac{kH}{R}\left(\sqrt{\zeta^2+^2} - \sqrt{\zeta'^2+R^2}\right)\right]\mathrm{sinc}\left[\dfrac{k\Xi}{R}(\zeta-\zeta')\right]}{\left[1 + \left(\dfrac{k}{a}\cdot\dfrac{\zeta-\zeta'}{R}\right)^2\right]\left[1 + \left(\dfrac{k}{aR}\right)^2\left(\sqrt{\zeta^2+R^2} - \sqrt{\zeta'^2+R^2}\right)^2\right]} \qquad (5.45)$$

provided a is large compared with the area of integration. Probably the simplest case to visualize is the Gaussian

$$_\gamma\varphi = e^{-\frac{a}{2}(\Delta\zeta^2 + \Delta\eta^2)}$$

which yields

$$_v\varphi = \Xi H\; \frac{e^{\frac{-\zeta^2 + \zeta'^2}{a}}}{a^2}\; \mathrm{sinc}\, \frac{kH}{R}\; \left\lbrack\sqrt{\zeta^2+R^2} - \sqrt{\zeta'^2+R^2}\right\rbrack\; \sin\left[\frac{k\Xi}{R}(\zeta-\zeta')\right] \qquad (5.46)$$

Finally, the coherent surface gives

$$_\gamma\varphi = 1$$

$$_v\varphi = H^2\Xi^2\, \mathrm{sinc}\left[\frac{kH}{R}\left(\sqrt{\zeta^2+R^2} - \sqrt{\zeta'^2+R^2}\right)\right]\, \mathrm{sinc}\left[\frac{k\Xi}{R}(\zeta-\zeta')\right] \qquad (5.47)$$

C. THE SIGNAL-TO-NOISE RATIO

Under the assumption that thermal noise dominates the process made in the derivation of the variance of $\hat{A}^2$, the ratio of the power in $\hat{A}^2$

to the variance of $\hat{A}^2$ is the signal-to-noise ratio. That is,

$$\frac{S}{N} = \frac{(A^2)^2}{\text{Var } \hat{A}^2} = \frac{A^4}{N_o^2} \iint |\varphi|^2 \, d\zeta \, d\zeta' \tag{5.48}$$

The autocorrelation function $_v\varphi$ calculated in section B can be used in the integral. For convenience, the expression will be normalized by N_o^2/A^4 and only the integral will be determined.

First, for the completely incoherent surface from Eq. 5.33

$$_\gamma\varphi = \delta(\rho)$$

$$|_v\varphi|^2 = \Xi^2 H^2 \, \text{sinc}^2\left[\frac{k\Xi}{R}(\zeta-\zeta')\right] \text{sinc}^2\left[\frac{kH}{R}\left(\sqrt{\zeta^2+R^2} - \sqrt{\zeta'^2+R^2}\right)\right] \tag{5.49}$$

Substituting for $N_o^2/A^4 \cdot S/N$,

$$\iint |\varphi|^2 \, d\zeta d\zeta' = \Xi^2 H^2 \iint \text{sinc}^2\left[\frac{k\Xi}{R}(\zeta-\zeta')\right] \text{sinc}^2\left[\frac{kH}{R}\left(\sqrt{\zeta^2+R^2} - \sqrt{\zeta'^2+R^2}\right)\right] d\zeta d\zeta'$$

$$\tag{5.50}$$

This is easily approximated for expansion along ξ by

$$\iint |\varphi| d\zeta \, d\zeta' \sim H^2\Xi^2 (\zeta_1-\zeta_0)^2 \quad \text{for} \quad \Xi, H \ll (\zeta_1-\zeta_0)$$

$$\sim H^2\Xi (\zeta_1-\zeta_0)^2 \quad \text{for} \quad H \ll (\zeta_1-\zeta_0) \; ,$$

$$\Xi < (\zeta_1-\zeta_0) \; ,$$

$$\text{and} \quad H < \Xi \tag{5.51}$$

Similarly, the coherent surface gives

$$\gamma^{\varphi} = 1$$

$$|_{v}\varphi|^{2} = H^{4}\Xi^{4} \ \text{sinc}^{2}\left[\frac{k\Xi}{R}(\zeta-\zeta')\right] \ \text{sinc}^{2}\left[\frac{kH}{R}\left(\sqrt{\zeta^{2}+R^{2}} - \sqrt{\zeta'^{2}+R^{2}}\right)\right] \quad (5.52)$$

so that

$$\iint |_{v}\varphi|^{2} \ d\zeta \ d\zeta' \sim H^{4}\Xi^{4}(\zeta_{1}-\zeta_{0})^{2} \quad \text{for} \quad H, \Xi \ll (\zeta_{1}-\zeta_{0})$$

$$\sim H^{4}\Xi^{3}(\zeta_{1}-\zeta_{0}) \quad \text{for} \quad H \ll (\zeta_{1}-\zeta_{0}) \ ,$$

$$\Xi < (\zeta_{1}-\zeta_{0}) \ ,$$

$$\text{and} \quad H < E \quad\quad\quad (5.53)$$

The Gaussian case is also instructive:

$$\gamma^{\varphi} = e^{-a(\triangle\eta^{2} + \triangle\xi^{2})}$$

$$|_{v}\varphi|^{2} = H^{2}\Xi^{2} \ \frac{e^{-\frac{\zeta^{2}+\zeta'^{2}}{a/2}}}{a^{4}} \ \text{sinc}^{2}\left[\frac{k\Xi}{R}(\zeta-\zeta')\right] \text{sinc}^{2}\left[\frac{kH}{R}\left(\sqrt{\zeta^{2}+R^{2}} - \sqrt{\zeta'^{2}+R^{2}}\right)\right]$$

$$(5.54)$$

If $1/a \ll H, \Xi$, then the sinc^{2} dominates the integral so that

$$\iint |\varphi|^{2} \ d\zeta \ d\zeta' \sim \frac{H^{4}\Xi}{a^{4}} (\zeta_{\eta}-\zeta_{1}) \quad\quad\quad (5.55)$$

This corresponds to a correlation area that is less than the size of the area δ. When compared with the completely coherent expression, it immediately follows that

$$\frac{H^{2}\Xi}{a^{4}} (\zeta_{1}-\zeta_{0}) < H^{4}\Xi^{3} (\zeta_{1}-\zeta_{0}) \quad\quad\quad (5.56)$$

as one would expect.

VI. REALIZATIONS OF THE ESTIMATOR

In this chapter we will show how the kernels derived in Chapter V may be realized. The form of the maximum-likelihood estimator

$$\int s\varphi^* s^* \, d\zeta \, d\zeta'$$

derived in the last chapter, is equivalent to the optimum detector for stochastic signal.[30,31,32] In the succeeding few paragraphs we shall lean heavily on the detection problem work but shall not follow it exactly, and we shall put it in a form better suited to our purposes.

It is convenient to have the form of the estimator in real variables. Breaking up the correlation function and signal into real and imaginary parts,

$$s = \xi + j\eta$$

$$\varphi = \Psi + j\Theta$$

(6.1)

we can easily show that our estimate becomes

$$\hat{A}^2 = \int_{t_1}^{t_1} \int_{t_0}^{t_1} \left[\xi(t)\xi(s)\,\Psi(t,s) + \eta(t)\eta(s)\,\Psi(t,s) + 2\xi\eta\theta(t,s) \right] ds \, dt$$

(6.2)

In obtaining this result, we have made use of the facts that

$$\text{Im} A = 0$$

and $\Theta = \Theta^*$ since ϕ is Hermitian.

There are several alternatives available for obtaining $\hat{A}^2$ other than direct calculation of the integral. Since in the development of φ we

always had an $e^{-jk(r-r')}$ factor, ψ will always contain $\cos k(r-r')$ and Θ the $\sin k(r-r')$. Denoting the other factors in Ψ and Θ collectively as $h(s,t)$, the kernel is

$$\xi(t)\ \xi(s)\ \cos k(r-r')\ h_\psi(t,s) + \eta(t)\ \eta(s)\ \cos k(r-r')\ h_\psi(t,s)$$

$$+ 2\eta(t)\ \xi(s)\ \sin k(r-r')\ h_\Theta(t,s) \quad (6.3)$$

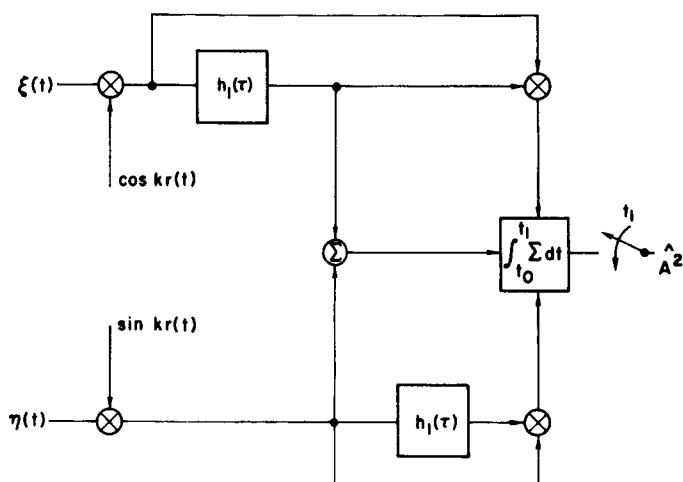Assuming that $h_1(t,s) = h(t-s)$, as it generally is from the previous section, the realization is

FIG. 32. FIRST REALIZATION, TIME INVARIANT
FILTER.

A second, more general, realization is given by Price and Green[32] from Middleton.[33] For this case, we must have an impulse response satisfying

$$h(t-\sigma) = \int h_2(\sigma',t)\ h_2(\sigma',\sigma)d\sigma' \quad \text{for all } t \text{ in } (a,b) \quad (6.4)$$
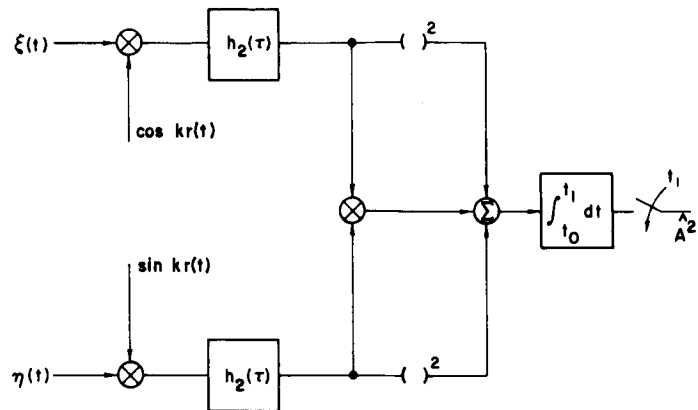
Then we have

FIG. 33.   SECOND REALIZATION, TIME-VARYING FILTER.

The third realization is the familiar weighted radiometer.   We require
a filter $h_3(\tau)$ so that

$$\left|H_3(\omega)\right|^2 = \int_{-\infty}^{+\infty} h(\sigma)\ e^{j\omega\sigma}\ d\sigma \qquad (6.5)$$
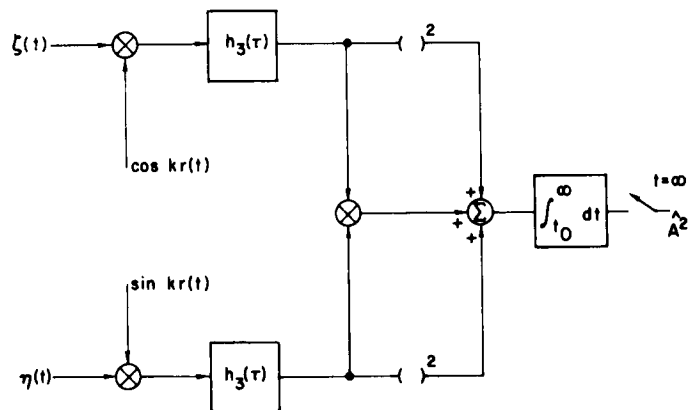
Then we have

FIG. 34.   THIRD REALIZATION, WEIGHTED RADIOMETER.

The fourth realization is in the form of three correlators followed by a special filter. The deviation follows directly from a change of variables in the double integral. Taking the first term as an example,

$$\xi(t) \ \xi(t') \ \cos k\big[r(t) - r'(t')\big]h(t-t') \qquad (6.6)$$

Changing variables

$$t - t' = \triangle$$
$$t + t' = \ell \qquad\qquad (6.7)$$

we have

$$\int_{\triangle = \frac{t_0 - t_1}{2}}^{\triangle = \frac{t_1 - t_0}{2}} \int_{\ell = t_0 + |\triangle|}^{\ell = t_1 - |\triangle|} \xi\left(\frac{\ell+\triangle}{2}\right) \ \xi\left(\frac{\ell-\triangle}{2}\right) \ \cos\left[k\left(\frac{\ell+\triangle}{2}\right) - r\left(\frac{\ell-\triangle}{2}\right)\right] h(\triangle) \ d\ell \ d\triangle$$

$$(6.8)$$

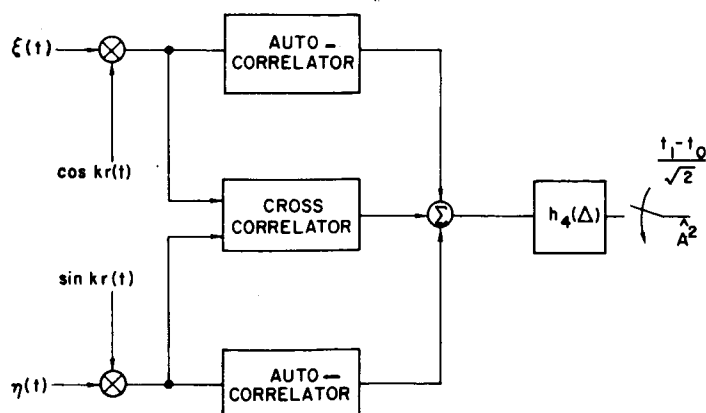which is achieved by the processor given below.

FIG. 35.   FOURTH REALIZATION, AUTO–CORRELATOR.

All of the above realizations may be achieved physically by means of regular filtering techniques or numerically with digital computation. This latter possibility offers considerable flexibility since the requirement of physical realization may be removed.

There is still at least one case of some interest left; this is the holographic or diffraction screen realization of the maximum-likelihood estimator. As an example, consider the situation in Fig. 36. This is
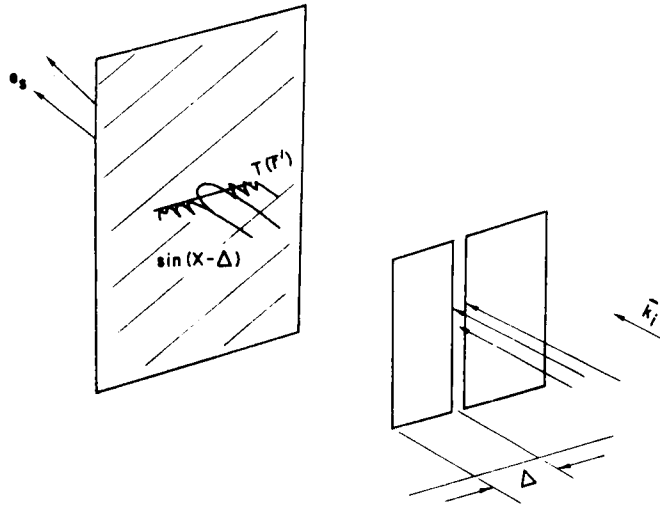

FIG. 36. FIFTH REALIZATION, OPTICAL ANALOG.

essentially Fig. 28 for the hologram reconstruction, except that the illumination has been modified with a slit so that an extra weighting function appears as a factor in the reconstruction integral. Supposing that the slit is adjusted to produce the familiar sinc (x) diffraction pattern, we have for the reconstruction

$$\left| \int e^{+jkr} \, g(x) \, \text{sinc} \, (x-\Delta) \, dx \right|^2 \qquad (6.9)$$

or

$$\int e^{-jk(r-r')} \, g(x) \, g(x') \, \text{sinc} \, (x'-\Delta) \, \text{sinc} \, (x-\Delta) \, dx \, dx'$$

which will be recognized as equivalent to the Middleton processor for a physically unrealizable filter.[33] The integration with respect to Δ may be achieved by moving the slit parallel to the data string at constant velocity and recording on photographic film. The film automatically squares and integrates.

VII. EXPERIMENTAL RESULTS WITH LUNAR ORBITER SPACECRAFT

A. NATURE OF THE EXPERIMENT

The first experimental tests of the application of bistatic-radar to celestial bodies were made in October 1966, and March 1967, using Lunar Orbiters I and III, respectively. These spacecraft carry a telemetry transmitter which, with appropriate filtering equipment on the ground, can be used as a source of continuous wave radiation on a wavelength of 13 cm. In addition, these spacecraft each have two antennas, a discone omni-directional antenna and a high-gain paraboloid, which can be arbitrarily oriented in space. Observations were made using both of these.

The radar parameters for the two cases are given below:

	Omni-Antenna	High-Gain Paraboloid
Radiated Power	100-mw CW	3-w CW
Antenna gain, transmitting	-1 db	22 db
Antenna gain, receiving	57	57 db
System temperature	80 °K	160 °K

The polarizations of the two transmitting antennas were not determined; the polarization of the receiving antenna is right-hand circular in the radio sense.

The receiving system temperature was largely dependent on the phase of the moon during the observations and this, along with certain constraints on the Sun, Earth, and spacecraft geometry for the use of the high-gain antenna, accounts for the differences in system temperature for the two cases.
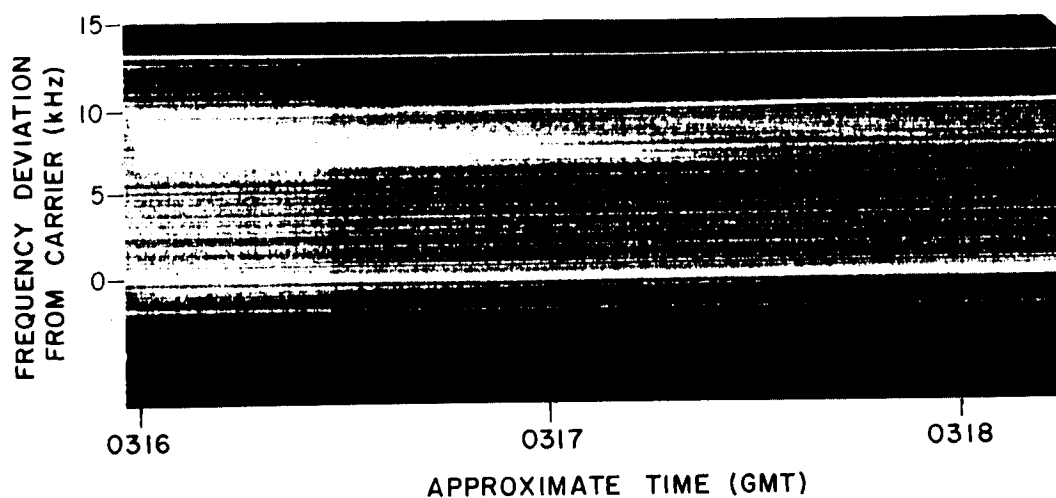
B. EXPLANATION OF THE OBSERVATIONS

Four examples of the records obtained are given in Figs. 37-40. These records represent spectra, measured with respect to the instantaneous spacecraft carrier frequency. Time advances to the right. Signal
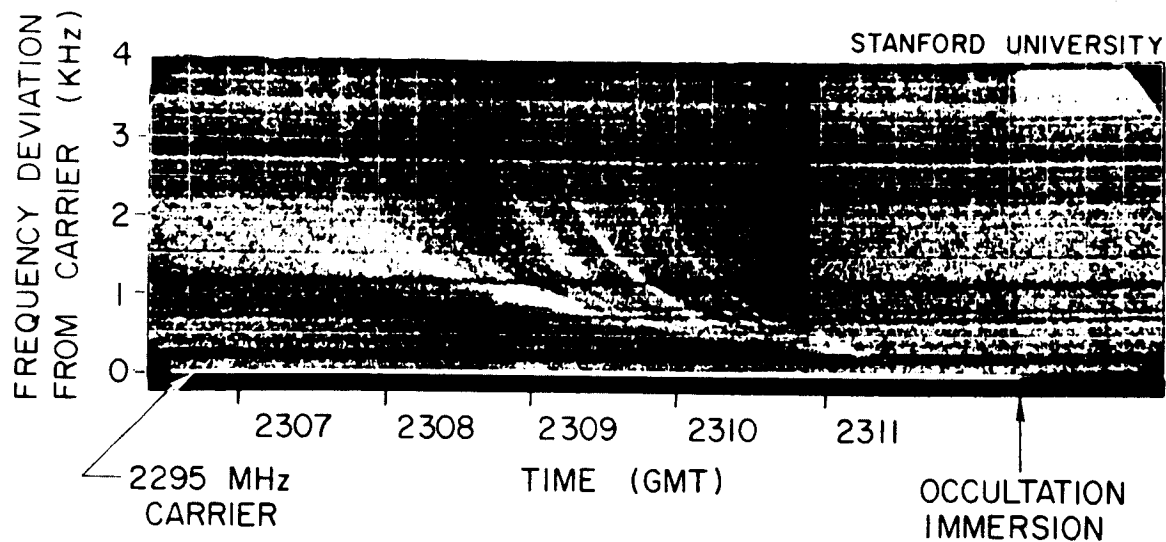
FIG. 37. TIME FREQUENCY TRACKS, LUNAR ORBITER I, 12 OCTOBER 1966, 23 GMT.

LUNAR ORBITER III 19 MARCH 1967
3W RADIATED POWER
HIGH GAIN ANTENNA

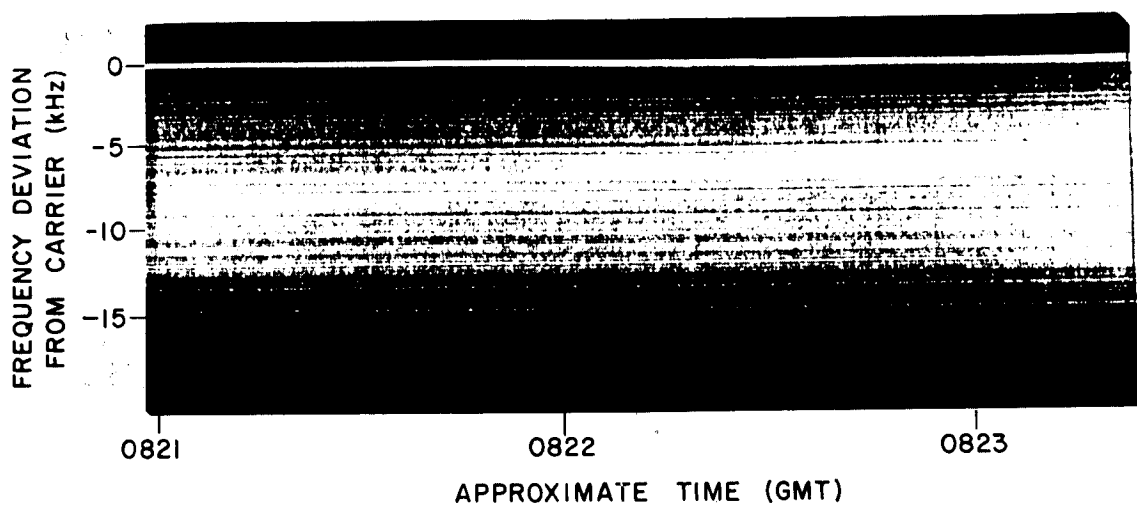FIG. 38. TIME FREQUENCY TRACKS, LUNAR ORBITER III, 19 MARCH 1967, 0300 GMT.
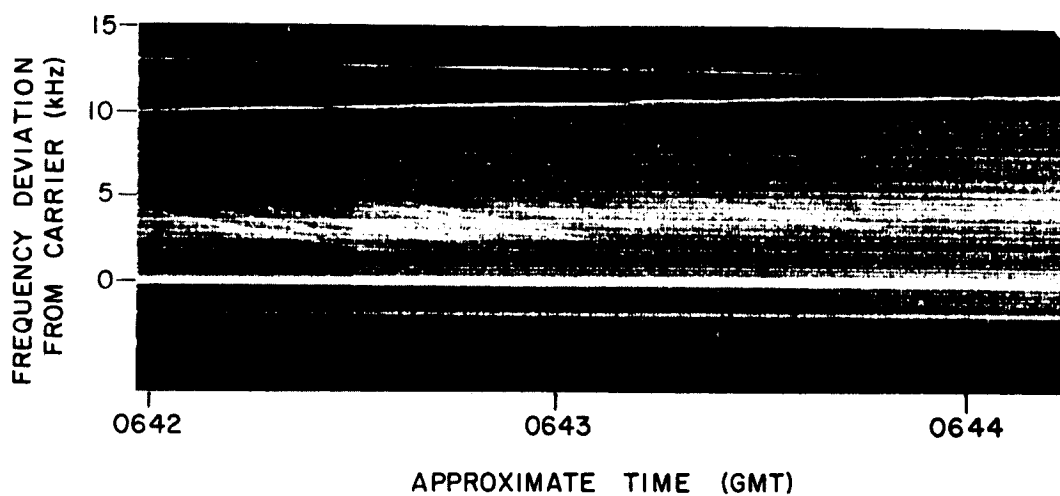
LUNAR ORBITER Ⅲ 19 MARCH 1967
3W RADIATED POWER
HIGH GAIN ANTENNA

FIG. 39. TIME FREQUENCY TRACKS, LUNAR ORBITER III, 19 MARCH 1967, 0600 GMT.

LUNAR ORBITER Ⅲ 24 MARCH 1967
3W RADIATED POWER
HIGH GAIN ANTENNA

FIG. 40. TIME FREQUENCY TRACKS, LUNAR ORBITER III, 24 MARCH 1967, 0800 GMT.

intensity is represented by relative shades of gray, with the strongest signals being white. The ordinate is frequency difference from the carrier in kHz. System noise appears as a speckled background, while the weak, continuous horizontal traces are due to imperfect filtering. The carrier frequency is the strong, continuous, horizontal trace appearing either near the top or bottom of the records.

The observations in Fig. 37 were made on 12 October 1966 while Lunar Orbiter I was approaching occultation immersion over the lunar crater Kastner on the eastern limb. Radiation was through the omni-antenna, and the radar parameters given for this condition apply. The altitude of the spacecraft was initially about 60 km, and decreased continuously to about 40 km during the period spanned by the record; its velocity was approximately 1.9 km/sec away from the Earth. Reflections from the surface appear as time-varying signals of decreasing frequency. (In this and the succeeding records, it is presumed, because of their continuity, that the persistent reflections are due to a fixed scattering center.) The spacecraft carrier disappears when the vehicle moves behind the limb at the time indicated as occultation immersion.

Figures 38 and 39 represent observations of Lunar Orbiter III made on two separate orbits on 19 March 1967. Radiation was through the high-gain antenna with the appropriate radar parameters. The antenna direction was to the side of the spacecraft's flight, and such that it intersected the moon with an angle of incidence of approximately 45°, and at a range of 600 km. The geometry was such that the received energy corresponds to oblique scattering. As one would expect from the development of Chapter II, the reflected energy is narrowly confined in frequency by the limits of the antenna beamwidth. Again, in Fig. 39, several discrete scattering centers stand out, and their progress through the antenna beam is easily followed in the frequency domain.

The conditions under which the records in Figs. 38 and 39 were made differ, in that the beam was directed at slightly different portions of the lunar surface. In the first, i.e., Fig. 38, the beam was directed at the crater Langrenus at the time the high-gain antenna was switched on, and the crater was then slowly carried out of the beam by the motion

of the spacecraft. Figure 38 is also of interest because the specularly reflected signals from the side lobes of the high-gain antenna are visible just below the carrier at the start of the record. For Fig. 39 the beam was directed to pass just south of Langrenus across an older region of the surface, which is composed primarily of maria.

Figure 40 gives observations under circumstances similar to those in Figs. 38 and 39, but the antenna was made to sweep an area of the Moon from the crater Albategnius near the center of the disk, south of Delambre, near Maskelyne and into the Mare Tranquillitatis. The features pointed out in Figs. 38 and 39 are present in this record as well.

C. REDUCTION OF OBSERVATIONS

The record in Fig. 37 has been used to demonstrate the nature of the two-dimensional information inherent in these observations. The frequency differences shown on the ordinate of these records are the instantaneous rate of change of phase with respect to the carrier, or direct signal. The quantity measured is

$$\Delta f = \Delta f_R - \Delta f_D$$

(7.1)

while

$$\Delta f_R = \frac{v}{\lambda} \sin \theta$$

The Doppler shift of the direct signal, Δf_D, may be calculated from the known orbit of the spacecraft, thus allowing the angle between the velocity vector and the vector to the target, θ, to be determined. Any given frequency offset therefore determines a cone about the velocity vector of half-angle θ, in which the scatterer must lie. The intersection of this cone with the surface of the Moon in turn defines a locus of points on the surface which might contain the scatter. The intersection of several loci, each determined from separate measurements on a single trace at different times, provides an estimate of the locations of the scatter on the lunar surface. It is a simple matter to show that this is equivalent to the use of a linear phase term for determining the azimuthal

position of the scatterer and quadratic term in the rate of change of phase to locate the scatterer in range, as suggested in Chapter III. While this represents an application of the idea presented in Chapter III, it is not a complete use of the method, since in this case we are using a number of estimates of instantaneous frequency rather than a filter matched to the entire record to obtain the results. Thus it has been demonstrated that two-dimensional information is present in the scattered spectrum, but the full potential of the method has not yet been realized.

Figure 41 is a drawing of Fig. 37 in which the traces have been identified by roman numerals. Figure 42 is a plot of the loci associated with trace III in Fig. 42 projected onto the $\eta\xi$ plane of the standard orthonormal selenographic coordinate system.[34] For purposes of illustration we show the intersection on only one side of the orbiter's ground track on the lunar surface. One division in Fig. 42 represents 17 km on the Moon. This particular record shows not only the locations of the scattering center responsible for the trace, but that the center itself is resolved into two different scatterers, one that contributes to the initial portion of the trace, and a second that comes into view near the end.

The locations of the scatters are given in selenographic latitude and longitude in Fig. 43 by the centers of the squares. The size of the squares depicts an estimate of the standard deviation of the intersections of the loci. These results have been published elsehwere, along with a preliminary analysis of the probable scattering mechanisms responsible for the observations.[35]
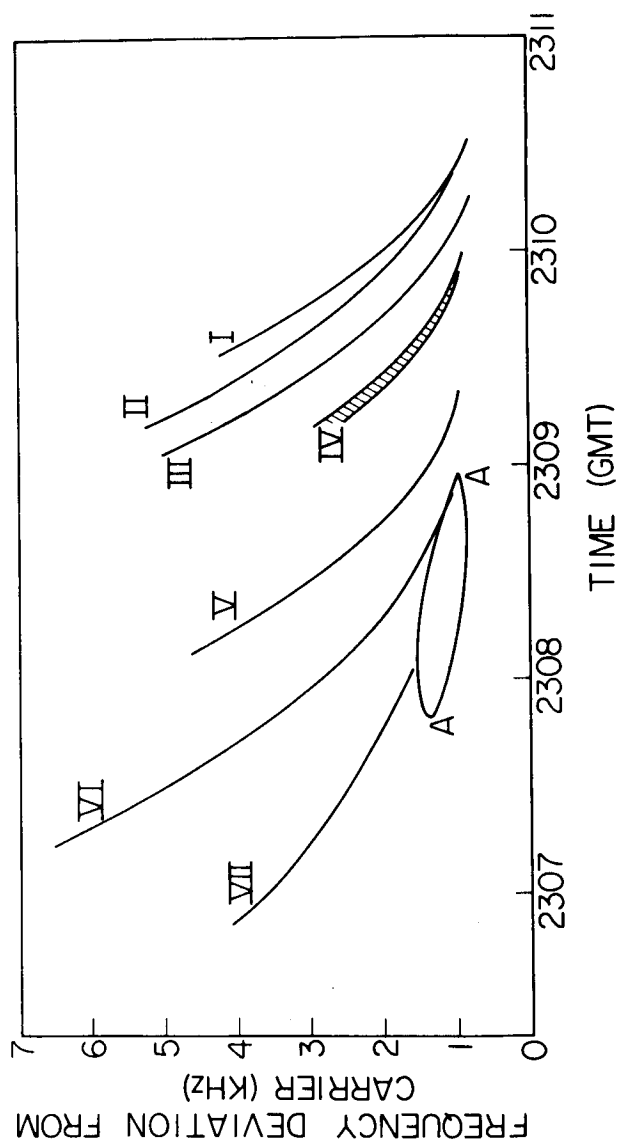
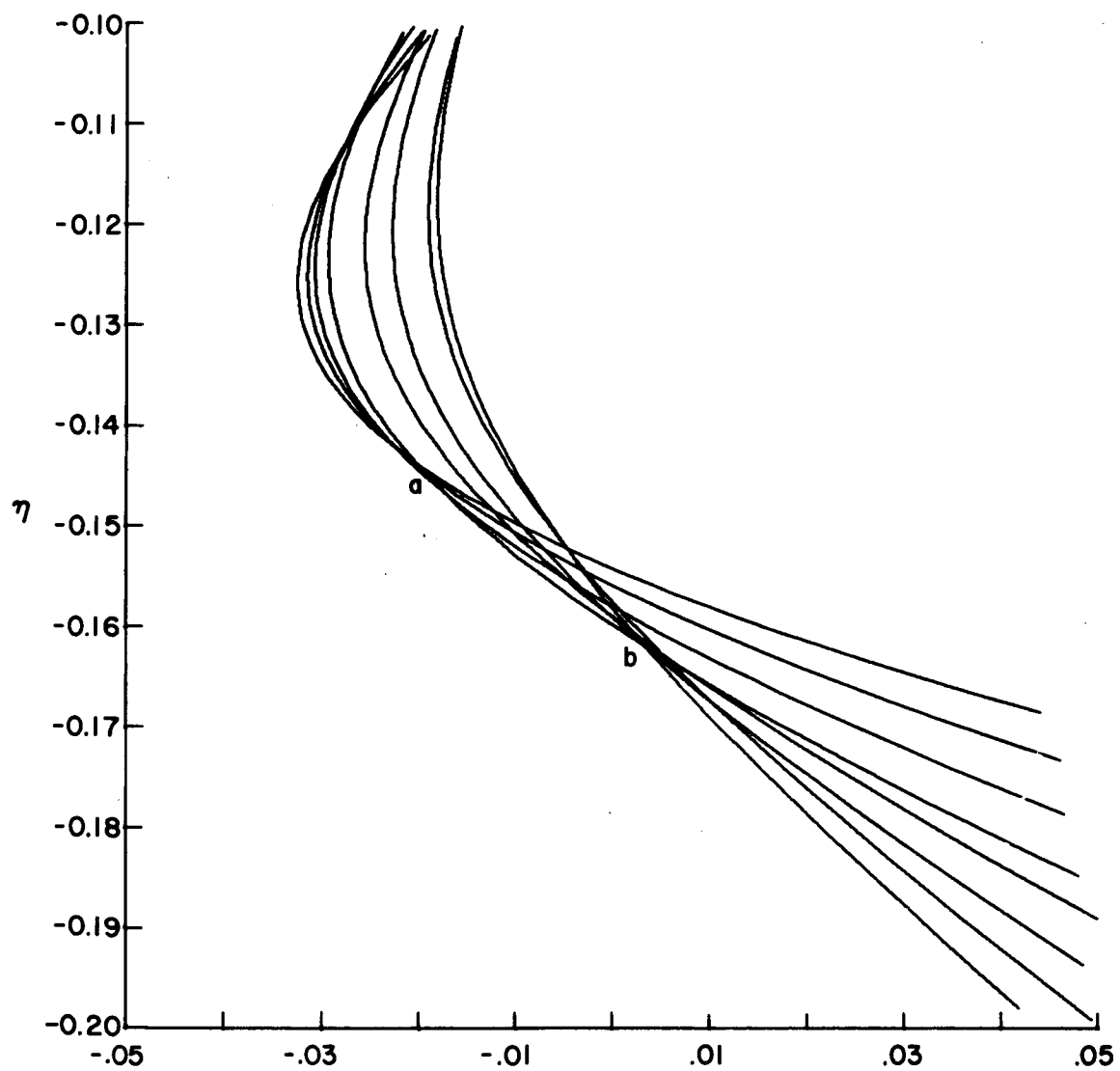FIG. 41. DRAWING OF TIME FREQUENCY TRACES FROM 12 OCTOBER 1966.

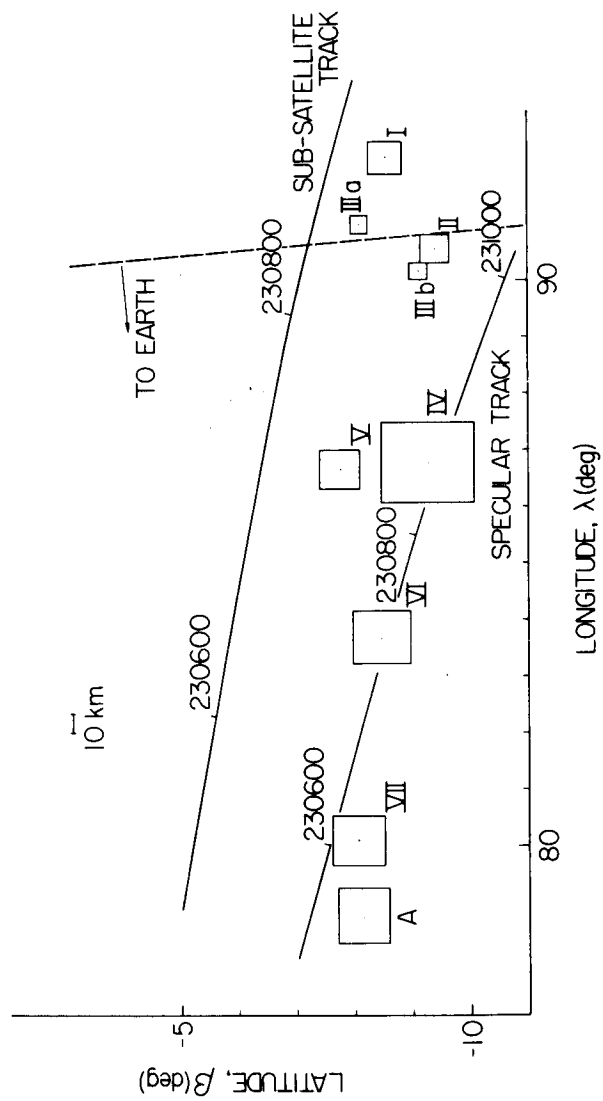FIG. 42. INTERSECTIONS OF LOCI OF CONSTANT DOPPLER SHIFT.

FIG. 43. LOCATIONS OF SCATTERING CENTERS IN TRUE SELENOGRAPHIC COORDINATES.

104

VIII CONCLUSIONS

In this study we have shown that astronomical bistatic-radars operating between a ground terminal and a vehicle in space may be used to probe and study planetary surfaces.

The illumination of a planet with radio waves produces a set of scattered fields above the surface, which, when compared directly with the incident wave, may be processed to produce a two-dimensional map of the radar brightness distribution of the surface of the planet. A crucial factor is the use of the indicent waves as a reference when obtaining the data on the scattered fields.

The resolution cell is variable in size and may be expanded to increase the signal-to-noise ratio at the output of the processor. But, for any given resolution cell, the inversions derived represent the highest signal-to-noise ratio--in the sense of minimum variance--that may be achieved with a linear system.

For a point source, the processor has analog interpretations as an array of antennas, a tracking filter, and a one-dimensional hologram.

The processor for an expanded resolution cell is realizable in a variety of ways, some of which represent physical filters, some of which do not.

The hologram analog may be modified to realize the processor in the case of certain special choices of geometry for the expanded resolution cell.

In practical terms, it would seem as though the methods for collecting and processing radar signals that have been given here can in fact achieve most of the advantages claimed for bistatic-radar in the introduction to this paper. If we consider the uplink case, a spacecraft instrumented with a relatively simple, narrow-band, phaselocked receiver, an antenna, some sort of data storage device, and telemetry readout is sufficient for this experiment. Large transmitters and antenna systems to provide the illumination are already in existence on the ground.

Depending on the choice of radar parameters, such an experiment would be expected to yield, in addition to its imaging features, data on surface and subsurface structure on the scale of a wavelength. With

further development of scattering theory and experiments along lines of research already begun, it may even become possible to deduce the composition of a surface from a remote measurement of its scattering properties.

In view of the difficulties associated with the optical mapping of Venus, the potential application of the imaging technique to the study of the surface of that planet is of special interest.

REFERENCES

1. Skolnik, M. I., <u>Introduction to Radar Systems</u>, McGraw-Hill, N.Y., 1962.

2. Skolnik, M. I., "An Analysis of Bistatic Radar," IRE Trans., ANE-8 19-27, March 1961.

3. Eshleman, V. R., "Radar Astronomy of Solar System Plasmas," SR No. 4, Stanford University, 1964.

4. Fjeldbo, G., "Bistatic-Radar Methods for Studying Planetary Ionospheres and Surfaces," SR No. 2, Stanford University, 1964.

5. Fjeldbo, G. and V. R. Eshleman, "The Bistatic-Radar-Occultation Method for the Study of Planetary Atmosphere," J.G.R. 70, 3217-3225, 1965.

6. Kliore, A. J. et al., "Occultation Experiment: Results of the First Direct Measurements of Mar's Atmosphere and Ionosphere," Science, 149, 1243-1248, 1965a.

7. Fjeldbo, G., W. Fjeldbo, and V. R. Eshleman, "Models for the Atmosphere of Mars, Based on the Mariner IV Occultation Experiment," J.G.R., 71, No. 9, 2307-2316, 1966.

8. Evans, J. V. and G. H. Pettengill, Memorandum to JPL Advisory Group on Radio Experiments in Space; Re: Bistatic-Radar Studies of the Moon, 23 January, 1961.

9. Eshleman, V. R. et al., "Bistatic-Radar Astronomy," Chapter 6 of Summer Study 1962 Review for Space Science Board NAS/NRC-1079, Iowa City, Iowa.

10. <u>Private communication by V. R. Eshleman</u>

    June 1960: Meeting on "Electromagnetic Studies of the Moon and Planets Using Space Probes," at Jet Propulsion Laboratory, Pasadena, California.

    June 24, 1960: "Conference on Planetary Atmosphere," Space Sciences Board of National Academy of Sciences, Arcadia, California.

    December 15, 1960 and February 2, 1961: "Conference on Planetary Atmospheres," Space Sciences Board of National Academy of Sciences, California Institute of Technology, Pasadena, California.

    February, 1961: Meeting of Ionospheric Physics Subcommittee of Space Sciences Steering Committee, NASA, Stanford, California.

11. Tyler, G. L. et al.: "Bistatic-Radar Detection of Scattering Center on the Surface of the Moon with Lunar Orbiter," In press, April 1967.

12. Helstrom, C. W., Statistical Theory of Signal Detection, Pergamon Press, New York, 1960.

13. <u>Ibid</u>, cf. Chapter II, Section 5.

14. Jackson, J. D., <u>Classical Electrodynamics</u>, Chapter 6, John Wiley and Sons, New York, 1962.

15. Born, M. and E. Wolf, <u>Principles of Optics</u>, Chapter 10, MacMillan, New York, 1964.

16. <u>Ibid</u>, Chapter 4.

17. Brouwer, D. and G. M. Clemence, Methods of Celestial Mechanics, Academic Press, New York, 1961.

18. Beckman, P. and A. Spizzichino, <u>The Scattering of Electromagnetic Waves from Rough Surfaces</u>, Chapter 7, Pergamon and MacMillan, New York, 1963.

19. Turin, G. L., "An Introduction to Matched Filters," IRE Trans. on Information Theory, 311-329, June 1960.

20. Sherwin, C. W. et al., "Some Early Developments in Synthetic Aperture Radar Systems," IRE Trans. ME, MIL-6, 111-115, April, 1962.

21. McCord, H. L., "The Equivalence among Three Approaches To Deriving Synthetic Aperture Array Patterns and Analyzing Processing Techniques," IRE Trans. ME, MIL-6, 116-119, April, 1962.

22. Cutrona, L. J., "A Comparison of Techniques for Achieving Fine Azimuth Resolution," IRE Trans. ME, MIL-6, 119-121, April, 1962.

23. Heimiller, R. C., "Theory and Evaluation of Gain Patterns of Synthetic Arrays," IRE Trans. ME, MIL-6, 122-129, April, 1962.

24. Tyler, G. L., "The Bistatic, Continuous-Wave Radar Method for the Study of Planetary Surfaces," J. Geophys. Res., 71, 6, 1559-1568, March 15, 1966.

25. Gabor, D., "A New Microscopy Principle," Nature, 161, 771, 1949.

26. Leith, E. N. and J. Upatnicks, "Reconstructed Wavefronts and Communication Theory," J. Optical Soc. Am., 52, 10, 1123-1130, October, 1962.

27. Courant, R. and D. Hilbert, <u>Methods of Mathematical Physics</u>, Vol. I, Interscience Press, New York, 1965, p. 138.

28. Helstrom, C., <u>Statistical Theory of Signal Detection</u>, cf. Chapter IV.C., Pergamon Press, New York, 1960.

29. Hofstetter, E. M., "Some Results on the Stochastic Signal Parameter Estimation Problem," IEEE Trans. Information Theory, IT-11, 422-429, July, 1965.

30. Helstrom, C., <u>Statistical Theory of Signal Detection</u>, cf. Chapter XI, Pergamon Press, New York, 1960.

31. Middleton, D., <u>Introduction to Statistical Communication Theory</u>, McGraw-Hill, New York, 1960.

32. Price, R. and P. E. Green, "Signal Processing in Radar Astronomy--Communication via Fluctuating Multipath Media," MIT Lincoln Laboratory TR No. 234, 6 Oct. 1960.

33. Middleton, D., "On New Classes of Matched Filters and Generalizations of the Matched Filter Concept," IRE Trans. on Information Theory, IT-6, 349-360, June 1960.

34. Yakovin, A. A., "Motion, Rotation, and Figure of the Moon," Ch. 1, From The Moon: A Russian View, ed. A. V. Markov, Univ. of Chicago Press, Chicago, Illinois, 1960.

35. Tyler, G. L. et al., "Bistatic-Radar Detection of Scattering Centers on the Moon Using Lunar Orbiter I," in press, March 1967.

DOCUMENT CONTROL DATA - R & D

(Security classification of title, body of abstract and indexing annotation must be entered when the overall report is classified)

1. ORIGINATING ACTIVITY *(Corporate author)*	2a. REPORT SECURITY CLASSIFICATION
Stanford Electronics Laboratories Stanford University, Stanford, California	Unclassified
	2b. GROUP

3. REPORT TITLE

BISTATIC-RADAR IMAGING AND MEASUREMENT TECHNIQUES FOR THE STUDY OF PLANETARY SURFACES

4. DESCRIPTIVE NOTES *(Type of report and inclusive dates)*

Scientific Report No. 19

5. AUTHOR(S) *(First name, middle initial, last name)*

George Leonard Tyler, Jr.

6. REPORT DATE	7a. TOTAL NO. OF PAGES	7b. NO. OF REFS
	109	35

8a. CONTRACT OR GRANT NO.	9a. ORIGINATOR'S REPORT NUMBER(S)
Grant NsG-377	
b. PROJECT NO.	Scientific Report No. 19
c.	9b. OTHER REPORT NO(S) *(Any other numbers that may be assigned this report)*
d.	SEL-67-042

10. DISTRIBUTION STATEMENT

11. SUPPLEMENTARY NOTES	12. SPONSORING MILITARY ACTIVITY
	National Aeronautics and Space Administration

13. ABSTRACT

The problem of imaging a planetary surface is considered from the point of view of continuous wave bistatic-radar in which transmissions originating on the Earth (or on a spacecraft) would be received on a spacecraft (or on the Earth) after reflection from a planetary surface.

An electromagnetic wave reflected by a planet may be considered as a superposition of the waves from elementary scatterers on the surface. Using a superposition model the ordinary radar brightness distribution, the differential radar cross-section, the polar scattering diagram, and the radar albedo of a surface are all related measures of the local surface properties.

The surface brightness distribution may be determined by cross-correlating the scattered fields (as measured by a spacecraft along some fraction of its trajectory) with the expected signal from each point on the surface. The predicted azimuthal resolution in wavelengths is inversely proportional to the angle subtended at the target point by the fraction of the trajectory over which the data are taken; in range the resolution in wavelengths is inversely proportional to the square of the same angle. The feasibility of the method depends on the use of the illuminating wave on board the spacecraft as a frequency reference to achieve the requisite stability.

Physical analogs of the process exist as modifications of holograms and synthetic antenna arrays. An additional analog is that of a bank of tracking filters, each of which is adjusted to receive the signals from a separate portion of the surface.

The maximum-likelihood estimator for the brightness of a specific scattering area, in the presence of white Gaussian noise at low input signal-to-noise ratios, is a

DD FORM 1473 1 NOV 65

14. KEY WORDS	LINK A		LINK B		LINK C	
	ROLE	WT	ROLE	WT	ROLE	WT
RADAR						
BISTATIC-RADAR						
IMAGING						
PLANETARY SURFACES						

Abstract (cont)

Hilbert quadratic form with the expected auto-
correlation function of the signal from the
scattering area as a kernel. For maximum res-
olution (minimum area) this is equivalent to the
cross-correlation method for obtaining the bright-
ness distribution. Furthermore, this estimate is
efficient in the sense of being unbiased and of
having minimum variance, for the low signal-to-
noise ratio case.
    The estimator may be realized with well-known
forms of time-varying or time-invariant filters,
or with correlators. A new realization is that of
a hologram scanned with a properly weighted illu-
minating wave.
    It is concluded that bistatic-radars operating
between a ground station and a vehicle in space
constitute a powerful technique with which to map
and to study planetary surfaces.